GROUND PENETRATING RADAR TECHNIQUE TO LOCATE COAL MINING RELATED FEATURES: CASE STUDIES IN TEXAS

A Thesis

by

NEELAMBARI SAVE

Submitted to the Office of Graduate Studies of
Texas A&M University
in partial fulfillment of the requirements for the degree of

MASTER OF SCIENCE

December 2004

Major Subject: Geophysics

GROUND PENETRATING RADAR TECHNIQUE TO LOCATE COAL MINING RELATED FEATURES: CASE STUDIES IN TEXAS

A Thesis

by

NEELAMBARI SAVE

Submitted to Texas A&M University
in partial fulfillment of the requirements
for the degree of

MASTER OF SCIENCE

Approved as to style and content by:

Mark E. Everett (Chair of Committee)	Brian J. Willis (Member)
Christopher D. Ellis (Member)	Richard Carlson (Head of Department)

December 2004

Major Subject: Geophysics

ABSTRACT

Ground Penetrating Radar Technique to Locate Coal Mining Related Features: Case Studies in Texas.

(December 2004)

Neelambari Save, B.S., Indiana University, Bloomington

Chair of Advisory Committee: Dr. Mark E. Everett

The goal of this research project is to identify the efficacy of the ground penetrating radar (GPR) technique in locating underground coal mine related subsidence features at Malakoff and Bastrop, Texas. The work at Malakoff has been done in collaboration with the Railroad Commission of Texas (RRC). RRC has been carrying out reclamation of abandoned underground coal mines at Malakoff since the early 1990's. The history of the specific mining operations (at Malakoff and Bastrop) that took place in the early 1900's has been difficult to ascertain; therefore, the use of a geophysical techniques like ground penetrating radar to identify hidden voids and potential subsidence features is vital for future reclamation process. Some of the underground mine workings at the field site have collapsed over time affecting the topography by creating sinkholes. GPR data, employing 25 MHz, 50 MHz and 100 MHz frequency antennae, have been collected in common offset patterns and azimuthal pattern. GPR data indicate the mine tunnels possibly connecting existing sinkholes by radargram hyperbolae that correspond with mine openings observed visually or during reclamation. This study also denotes the importance of understanding the variable

physical properties of the stratigraphy, which could lead to false alarms by misinterpretation of the radar signals. Natural and man-made above-ground structures cause obstructions in data collection, and hence an optimal design is required for each survey. RRC successfully ground-truthed the data during its reclamation process. In turn, the acquired geophysical data helped to guide the reclamation. At Bastrop, GPR data along with historical documentation led to the conclusion that coal mining did exist in this region but is not a major concern to the immediate stability and safety of the field site. It can be concluded from both the studies that the GPR technique identifies anomalous shafts/tunnels possibly connecting potential failure.

ACKNOWLEDGEMENTS

I would like to thank my advisor Dr. Mark E. Everett for his constant and continued support and guidance.

I would like to express my gratitude to Mr. Jon Brandt and Mr. William Reimer from the Railroad Commission (RRC) of Texas for providing the field sites, geologic and background information. I would also like to thank Dr. Brian J. Willis and Dr. Christopher D. Ellis for their input and comments on the thesis material.

Special thanks to the Henderson family (Malakoff, TX), Sims family (Bastrop, TX), and the Cavender family (Bastrop, TX) for allowing me to use their land for data collection.

I would also like to thank Carl Pierce for his equipment related help and field assistance. Rain or shine, Jamie Collins, Luke Cooper, Eyal Hakim, Shantanu Singh, and Ramesh Save assisted me in completing my surveys and I am grateful to them for the assistance.

I would also like to acknowledge and thank the Department of Geology & Geophysics at Texas A&M University for the equipment and for the assistance in arranging for the field work.

Finally, I would like to express gratitude towards my parents without whom reaching this far would have been impossible.

TABLE OF CONTENTS

Page

Page

LIST OF FIGURES

FIGURE Page

FIGURE Page

FIGURE Page

LIST OF TABLES

TABLE Page

INTRODUCTION

The main objective of this research project is to identify and investigate how well ground penetrating radar (GPR) performs in characterizing near surface coal mine related features. Coal mining in the Eocene – Paleocene Wilcox Formation (Fisher, 1963) was carried out at Malakoff (near Dallas), Texas and Bastrop (near Austin), Texas in the first half of the 20th century: generally during the period from 1905 to 1940. Most of the mining operations were underground even for shallow excavations ($\leq$ 5 m) due to a lack of surface mining techniques. Unfortunately, few maps or records survive describing these abandoned mine workings. Today, many of these underground coal mining locations are residential zones. This research describes efforts to identify non-invasively mine workings in pastures and a residential setting at Malakoff and Bastrop, respectively. Land subsidence due to the coal mine workings can be hazardous to occupants and livestock and can cause property damage. Coal mining related surficial features can also reduce the value of the property and hence it is important from an economic perspective to map these features. Subsidence due to karst topography or due to underground mining is a common problem in many parts of the world. Hence, it is also important to understand the natural (geologic) and human induced factors which lead to sinkhole formation. Geophysics provides non-invasive techniques to investigate sub-surface features by detecting spatial contrasts in physical properties of the soil, as well as buried objects and void spaces.

This thesis follows the style and format of Geophysics.

The findings of this research have been used to guide reclamation of abandoned coal mining sites at Malakoff, which in turn provided ground truth for a posteriori evaluation of the geophysical data. GPR mapping helps to assess the risk associated with coal mining subsidence.

The field sites at Malakoff and Bastrop are similar with respect to geomorphology, the extent of mining, and socio-cultural electromagnetic interference, but there are several differences. It is important to identify and understand the natural and man-made constraints at each site that deter the design of an ideal survey and accurate interpretation of the radargrams. Azimuthal as well as linear GPR data acquisition schemes can be restricted by obstacles such as sinkholes, trees, fences, buildings and other natural or man-made features. A novel azimuthal data acquisition technique is used in this study to detect possible connections between different subsurface excavated rooms. This information is used to identify the future risk of subsidence of these rooms. Data acquisition can also be restricted by the type of GPR antennae used, the sub-surface lithology and the physical properties of this lithology.

COAL MINING IN TEXAS

Coal is a product of plant remains that have been compacted, hardened, chemically altered, and metamorphosed by heat and pressure over geologic time. Coal forming plants are buried in a swampy oxygen-poor ecosystem, where the low oxygen levels prevent complete decomposition of the plant remains. Subsequently, the reduced organic matter is transformed into coal. Most of the coal mined today formed during the Carboniferous era (280 - 345 Ma).

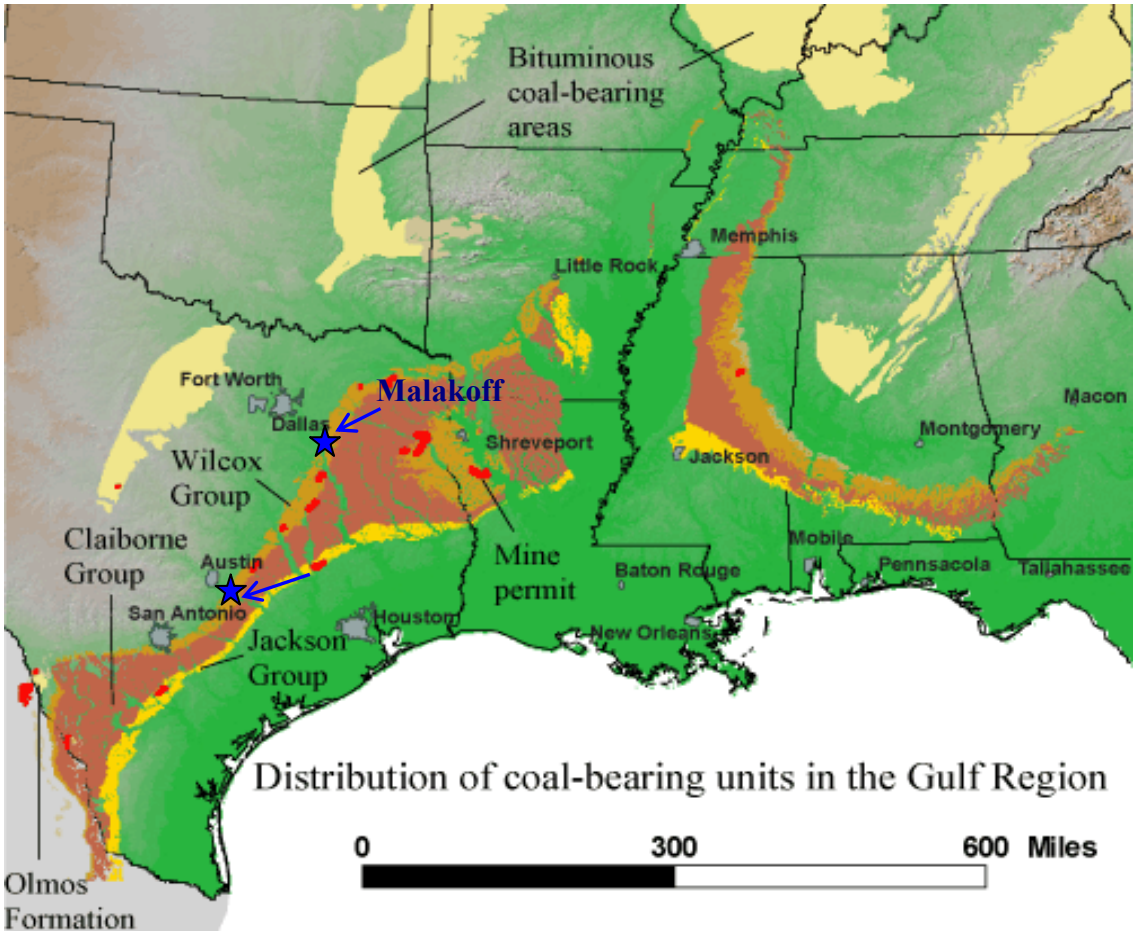

Fig. 1. Location of Malakoff and Bastrop, Texas. Field site location on coal-bearing units in the Gulf Region of Texas. (Map: National Coal Resource Assessment, USGS)

Classification of coal is based upon the intensity and duration of the geologic processes which have affected the sediments. The classification from low intensity - short duration to high intensity - long duration is:

Peat ➔ Lignite ➔ Bituminous Coal ➔ Anthracite ➔ Graphite.

In Texas, the late Eocene period was dominated by cycles of transgressive - regressive marine sediment deposition. These cycles were separated with intervals of non-marine sedimentation and bedding of volcanic ash (Yancey, 1995). Lignite outcrops in some of these intervals in association with deltaic and coastal plain sediments. Trending northeast-southwest in east central Texas (Fig. 1), the Wilcox group (coal bearing formations at Malakoff and Bastrop) occurs near the surface beneath Quaternary alluvium in a broad belt roughly parallel to the Texas section of the Gulf of Mexico coastline (Mathewson, et al., 1980). The Wilcox group is divided into three formations in east Texas: from the lowest unit to the highest, these are the Hooper Formation, the Simsboro Formation and the Calvert Bluff Formation (Middleton and Luppens, 1995). Middleton and Luppens (1995) estimate the thickness of the Wilcox group to be 365 to 1,060 m in east-central Texas.

PAST, PRESENT, AND FUTURE OF US COAL MINING

Coal Production

With the introduction of the railroad, coal mining was developed as a means to provide fuel for the trains. The first written records of coal mining in the US are found from 1819 (Mathewson, 1980). The total US coal production in 1880 was ~ 20,000 tons. The gradual development of oil fields reduced the dependence on coal as a source of energy and hence its production. The country saw a renewed interest in coal production during the 1970's oil crises as is evident from Fig. 2. Coal production declined again in 2002 and 2003, probably because of a slow down of the economy.

Some of the negative factors that affected production in early 2003 are expected to change in 2004 due to increased coal demand. Factors like high natural gas prices and continued economic recovery are responsible for the increased demand predicted for 2004 and beyond (Annual Coal Report, 2003). The US Department of Energy 's (DOE) Strategic Center for Coals (Overview, 2004) emphasizes the importance of developing advanced technologies and improving scientific knowledge regarding coal production in order to enable economic prosperity and strengthen the energy security of the nation by reducing the dependence on imported oil, while avoiding environmental costs by using effective pollution control technologies.

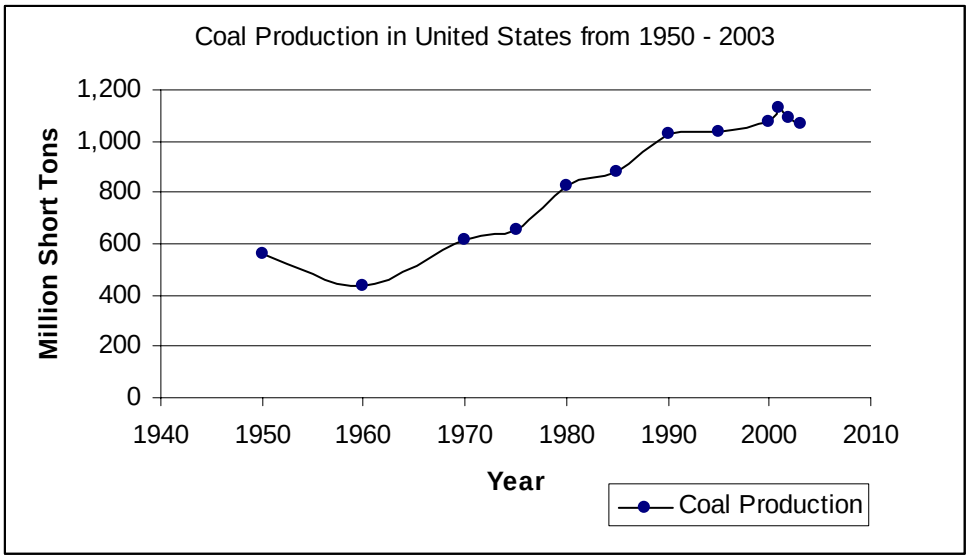

Fig. 2. Coal production in US from 1950 to 2003 (Mathewson, et al., 1980; US DoE Strategic Center for Coals (Overview, 2003)**.**

Mining Subsidence

Coal production has been increasing steadily since the 1970's and the prospects of coal mining in the United States in the future look promising since coal is a domestic source of energy. Present rules and regulations help to prevent current mining operations from later developing into hazardous situations. But past underground coal mining, which were mainly room and pillar method were less regulated, can give rise to conditions which are hazardous to the property and life. Some of the consequences of underground coal mining are: disturbance of the surface leading to possible subsidence; pollution of surface and ground water; and spontaneous ignition leading to fires in the cavities (Dunrud and Osterwald, 1980).

While there exists a lack of information about mining activities from the early 20th century, it is important to understand the process and factors that lead to mine subsidence. The Ohio Department of Natural Resources, Division of Geological Services (Crowell, 2001) describes some of the factors controlling mine subsidence as: height of mined out area, width of the mine, thickness of overburden, strength of bedrock, hydrogeology, fracture/joints and time. The deeper the mine, the longer the time for it to collapse, though the larger the surface area affected. Fluctuation of water circulation in the mine weakens the roof rock so that it could collapse if unsupported. As the roof sags, it ruptures and caves into the mined out area. The roof rock then fragments, crumbles, rotates and is deposited, as incompletely compacted fill (Fig. 3). Existence of fractures and joints increases the likelihood of the subsidence. As a result of

the complexity and the variability of different aspects related to mine subsidence, the time a mine can take to collapse can not be predicted with much certainity.

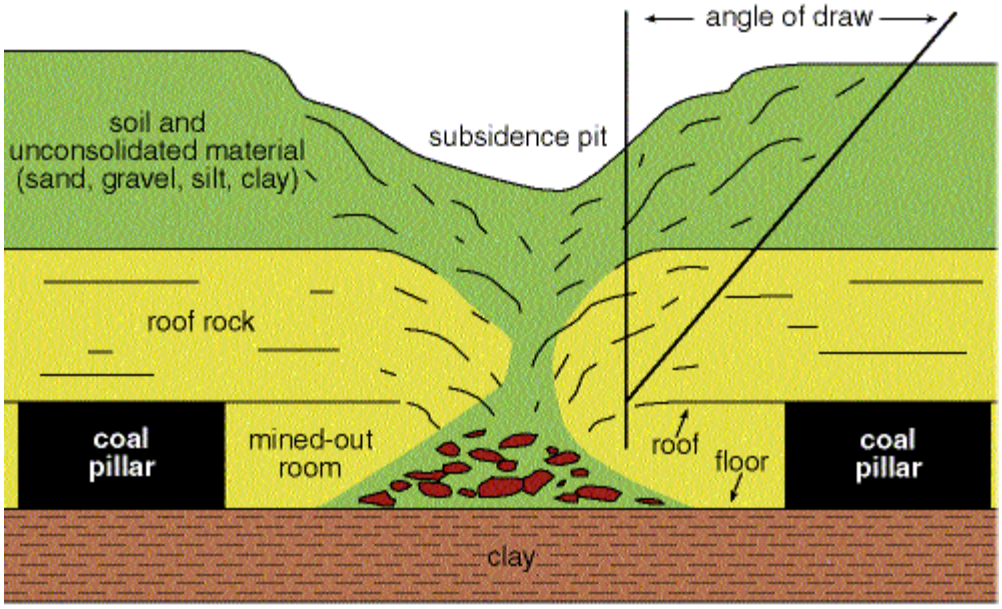

Fig. 3. Coal mining subsidence. Typical subsidence emerging from mine roof collapse resulting into a sinkhole formation (Source: Ohio Department of Natural Resources).

PREVIOUS STUDIES

A number of geophysical techniques have been used to detect void spaces. Micro-gravity easily detects the anomalies due to spatial variation in the density of the void space and surrounding host material. Magnetic anomalies are caused by variation in magnetic properties of the subsurface. Resistivity tomography can also be used since it detects anomalies generated by the spatial variation in electrical resistivity of the target verses the surrounding. The resistivity of the void space is higher than the resistivity of the host material. These techniques are adequate if general information about the void or anomaly is available, but it can be difficult to detect unknown voids or anomalies (Chamberlain, et al., 2000). All these techniques can locate the anomaly but do not identify the exact location of the anomaly and require a significant amount of processing.

Some recent studies that use GPR for subsurface void investigation are: surveys of potential sinkholes, underground storage tanks, underground vaults (Mellet, 1995); survey of buried sinkhole at Ghor al Haditha, Jordan showing buried sinkholes indicating deeper hydraulic activities (Batayneh, et al., 2002); detection of caves in limestone for archaeological and palaeontological investigation (Chamberlain, et al., 2000); study of karst features and the associated topography at Herault, France (Al-fares, et al., 2002). Many other such studies exist in the applied geophysics literature.

Ground penetrating radar uses electromagnetic wave propagation and scattering to image and locate changes in electrical and magnetic properties of the ground. Likely underground mine void spaces or tunnels (Fig 4(a)) are typically represented in GPR

sections (radargrams) as two parallel, concave—upwards hyperbolae cresting at the top and bottom of the mine workings (Powers and Ohloeft, 1996). Following to the discussion in Davis and Annan (1989), the radargram in Fig. 4(c) represents the idealized GPR signature of the anomalous zone shown in Fig. 4(b). The reflections are governed by the electrical properties of the media through which the radar waves propagate. The antennae's are sensitive to see the anomalous zone prior to arriving over it (as seen in Fig. 4(b)), resulting in hyperbolic reflections (as seen in Fig. 4(c)). Further details and the theory of the radar are discussed later.

Fig. 4 GPR anomaly. **(a)** Example of a mine addet (shaft opening into a tunnel) opening at Malakoff, **(b)** Conceptual illustration detection of an anomaly using GPR. (From Davis and Annan, 1989), **(c)** Conceptual illustration of GPR radargram being used to detect an anomaly.

(b)

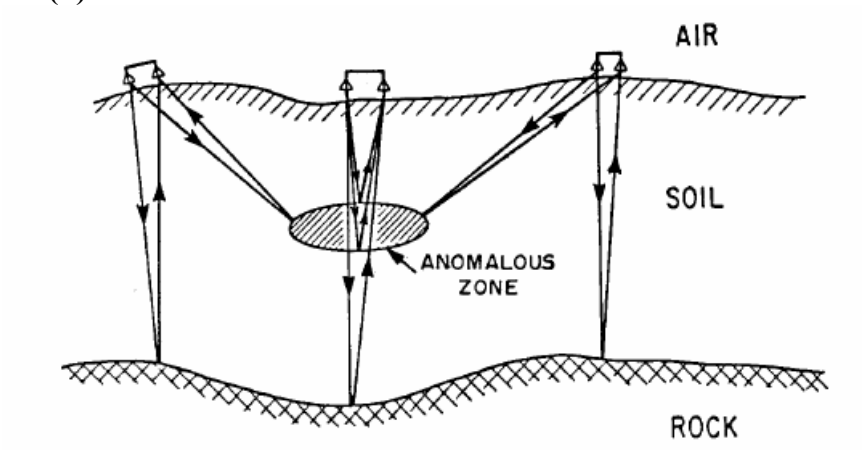

(c)

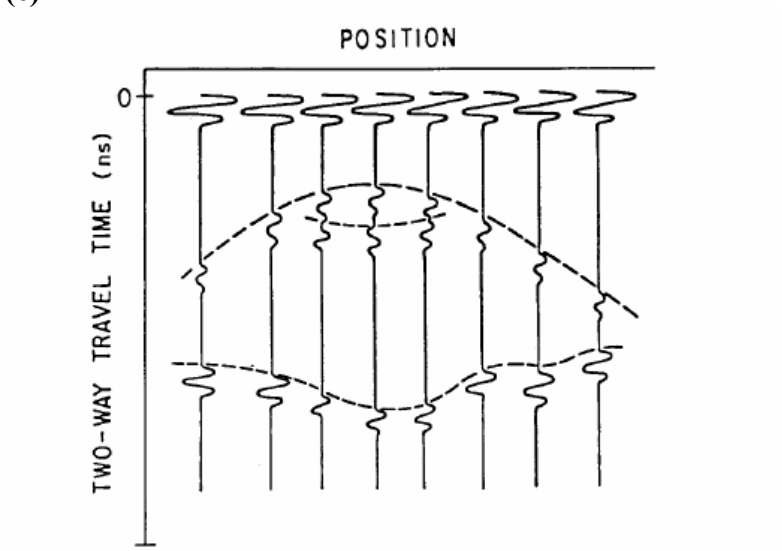

Fig 4. Continued

Field studies indicate that radar wave behavior is influenced by water content, physicolo-chemical characteristics of pore water, solid-liquid-air proportion, and

structure and void ratio of the solid phase (Carreon-Freyre, et al. 2003). Multiple reflections are commonly found in GPR data. These are recognized by their lower amplitude owing to attenuation and somewhat discontinuous nature due to multiple scattering of the waves. Shallower anomalies result in many strong multiple reflections whereas the deeper anomalies result in fewer weaker multiple reflections (Friedel, et al., 1990). It is also noticed that coarse material lenses occurring within a stratigraphic layer such as silt create radar patterns which look chaotic (Beres, and Haeni, 1991). Further more, according to Carreon-Freyre (2003), increase in water content in such varied grain size lenses enhance the contrast in the signal and hence can aid in identification of an anomaly. Near surface boulders can lead to hyperbolic diffraction patterns (Beres, and Haeni, 1991,). A void space could also possibly create a bow-tie like feature and a velocity pull-up or pull-down depending upon the velocities of the media through which the EM wave propagates (Powers and Olhoeft, 1996).

At Malakoff and Bastrop, the underground coal mine rooms were connected by tunnels or shafts. These tunnels or shafts today are either void spaces or void spaces filled with sediments that have been washed in. In both cases there is a material property contrast with the surrounding host sediments. The tunnels or shafts act as point radar reflectors and generate hyperbolic move out in the radargram. Many of the radargram features discussed in the previous paragraphs were observed in the GPR data from Malakoff and Bastrop sites.

FIELD SITE DESCRIPTION

Malakoff

The Rail Road Commission of Texas (RRC) has been carrying out reclamation of abandoned underground coal mines at Malakoff since the early 1990's.

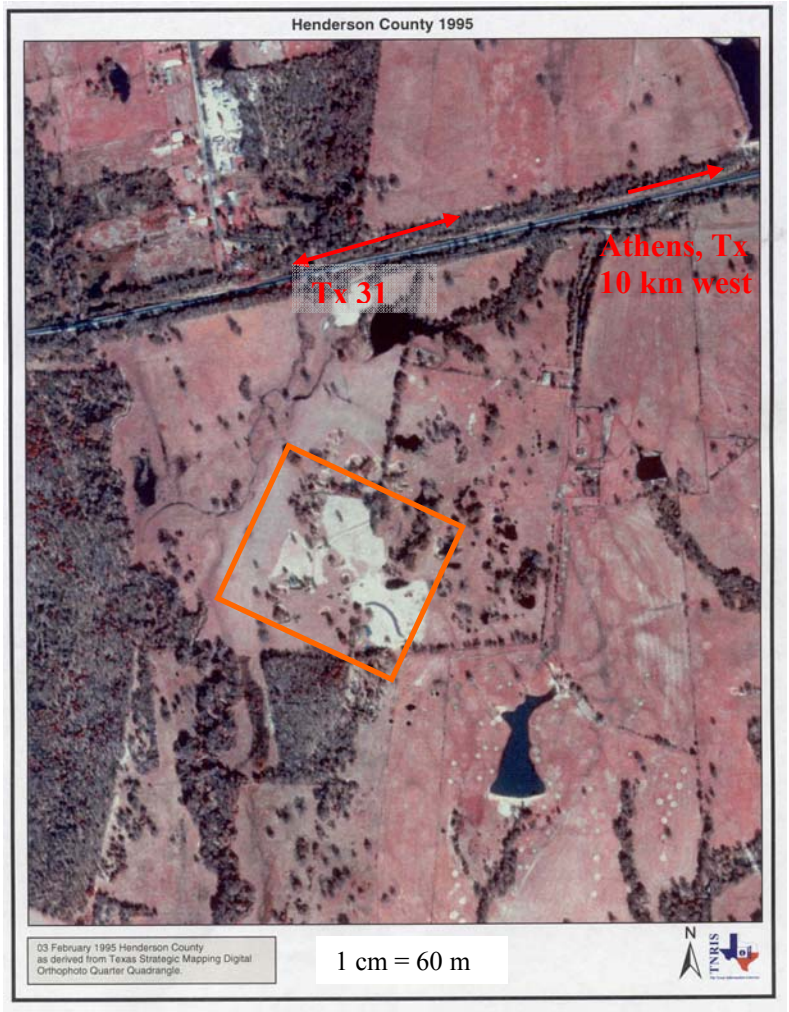

Fig. 5. Aerial photograph of the Malakoff, Texas, field site (TNRIS)

The landscape at the field site (Fig. 5) is rolling hills with a moderate-relief underlain by Paleocene – Eocene Wilcox Group deposits: Indio Formation (~ 21 m thick) below which lies the Wills Point Formation. The lithology mainly consists of thin-bedded and laminated, moderate to fine grained sand and some shale. There are common massive clay layers and lenses of sandstone with few beds of lignite. The soil is poor to moderately well drained and the permeability is low to moderate, hence the water capacity is medium to high with varying erosion. The coal seams around this area are 2.0-3.0 m thick (Fisher, 1963). A detailed history of the lignite coal mining operations that took place in the 1920s and 1930s has been difficult to ascertain; therefore, the use of a geophysical technique like GPR to identify hidden voids and potential subsidence features is an important component of the reclamation process. Some of the underground mine workings have collapsed over time and have created sinkholes as deep as 10-12 m with varying diameter (but at least ~ 3 m wide). By early 2003, there were at least 10 collapse features at the site enclosed by the orange rectangle in Fig 5. These were identified as high priority for reclamation by the RRC.

Malakoff: Previous Reclamation Work

More than 9 Texas coal sites have been reclaimed by the Abandoned Mine Land (AML) program since 1980 (*Re-inventory of abandoned coal mines in Texas, 1995*). The main criterion for prioritization of reclamation work, as defined by RRC, is the protection of public health, safety, general welfare, and property from extreme danger due to adverse effects of coal mining practices. Priority is given to sites that are in the immediate vicinity of a residential area in which coal mining has already had an adverse impact upon a community.

Previous reclamation and restoration work in 1994 was conducted by RRC at the Henderson's property at Malakoff. Since then, global positioning system (GPS) observations have been used to record the subsidence and location of new collapse features. Physical characteristics such as variations in vegetation, fresh collapses, creep in the soil, etc., were also noted as they are good indicators of fresh subsidence or future failure zones. Taking into consideration the main criterion for prioritization, 10 sinkholes (one of them seen in Fig. 6) were marked for reclamation in the summer of 2003 at the Henderson's property by the RRC (Fig. 7). Information regarding the dimensions of these high priority sinkholes which were surveyed using GPR is provided in Table 1. The rows highlighted indicate the sinkholes that are studied in this report using GPR.

Table 1. Sinkhole dimension information for Malakoff field site. Adapted from Railroad Commission of Texas Invitation for Bids for Malakoff Underground II Abandoned Mine Land (AML) site (FY 2003)

Sinkhole	Approximate Width and Length (m)	Approximate Depth (m)	Approximate Volume (cu. m.)	Comments
S-1	12 x 9	2	157	
S-2	12 x 11	2	318	Holds water
S-4	8 x 6	2	100	
S-5	8 x 6	5	323	
JBR-10	8 x 7	2	158	Holds water
JBR-16	11 x 7	3	77	May have water
JBR-19	13 x 13	2	154	
JBR-26	12 x 12	2	19	Holds water
JBR-29	8 x 8	2	106	Holds water
JBR-30	2 x 2	1	5	
		Total	1419	

Note: Sinkholes highlighted in the table were surveyed using GPR

Fig. 6. Surficial subsidence features (sinkhole) at Malakoff. Mr. William Reimer in (high priority) Sinkhole S-4 at Malakoff, Texas (Source: RRC Texas)

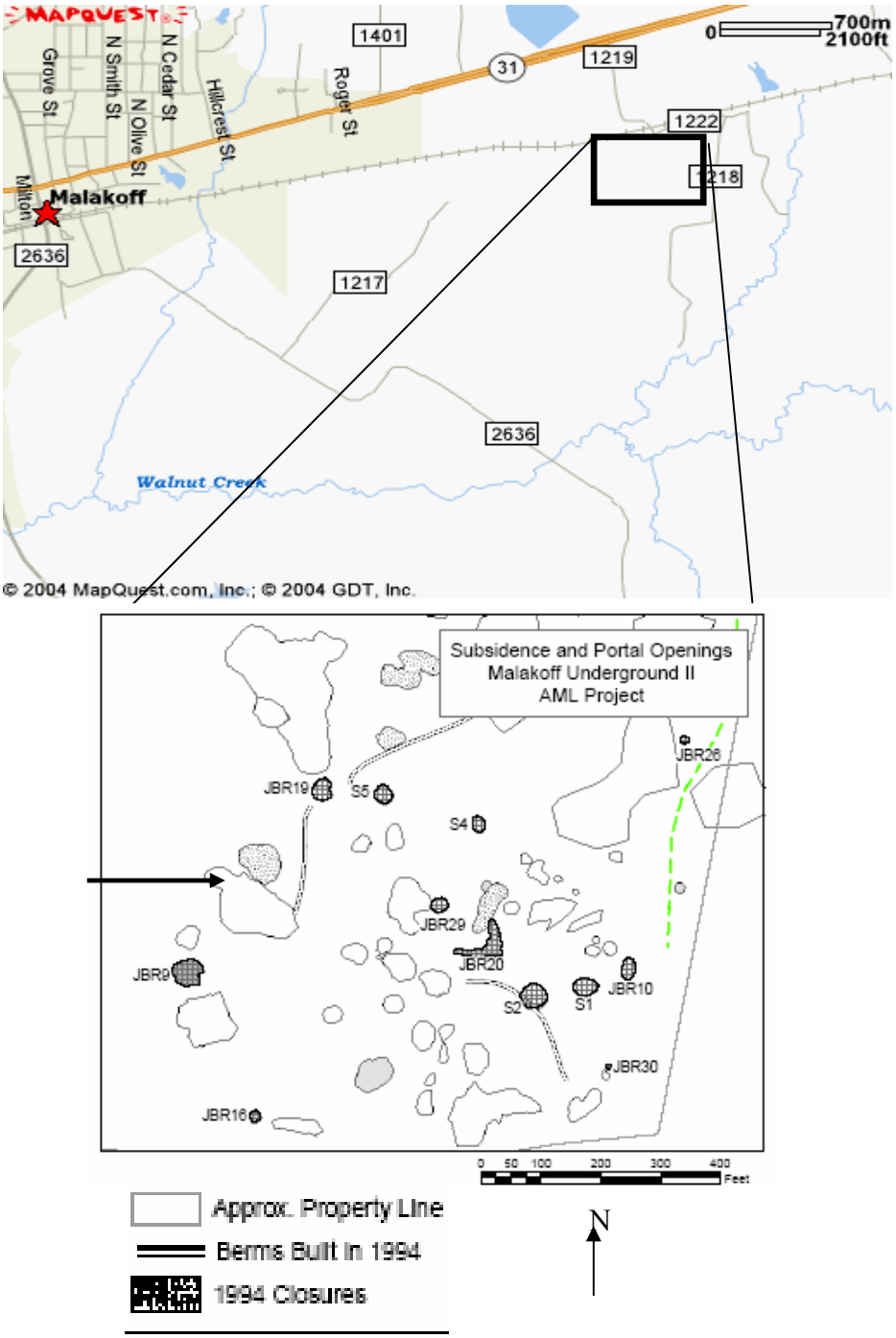

Fig. 7. Location of subsidence features (on Henderson's property), Malakoff field site (Mapquest.com and RRC, Malakoff Underground II AML Project invitation for bids).

Bastrop

Following the survey at Malakoff, with the help of RRC, we identified another field site at Bastrop, Texas. This field site (Fig. 8) is in a residential area located along the Colorado River floodplain near the town of Phelan in Bastrop County, Texas.

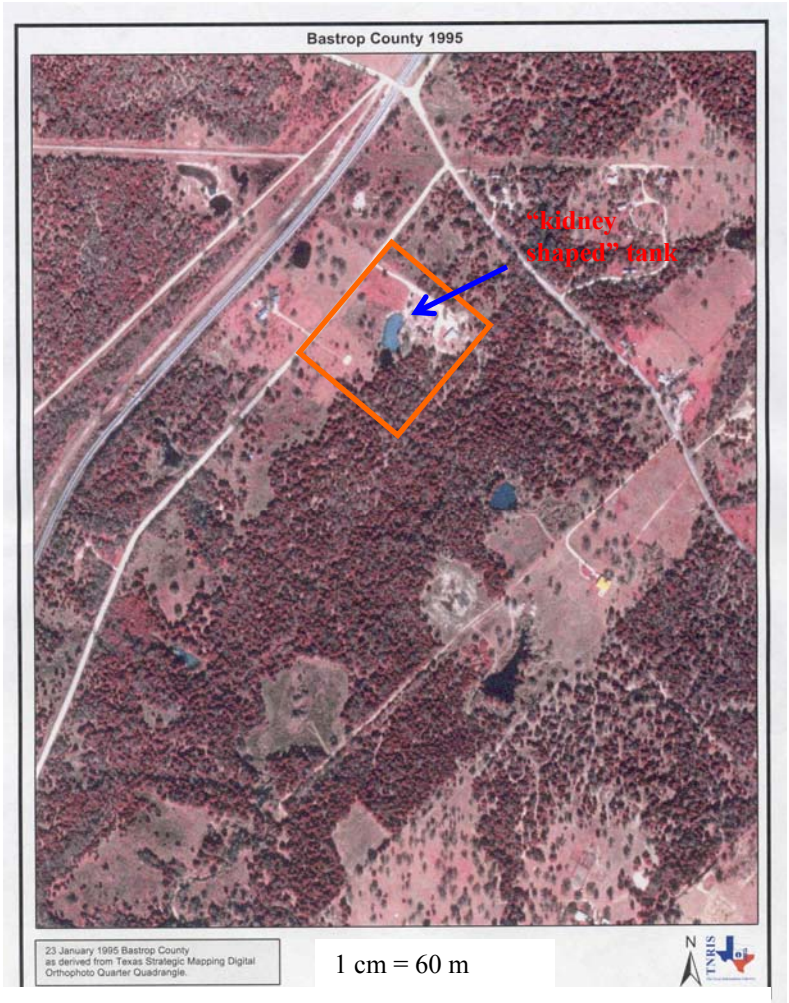

Fig. 8. Aerial photograph of the Bastrop, Texas, field site (Source: TNRIS)

The property owner was unaware (before the property was purchased) of the earlier coal mining in the immediate area. The field site is underlain by Paleocene – Eocene Wilcox Group: Calvert Bluff Formation (~ 21 m thickness) below which lies the Simsboro Formation. The ground surface is mostly terrace and stream alluvial deposits with rounded pebbles and cobbles, of generally moderate to fine sandy loam texture. The permeability of the soils is low; hence the movement of water and air is restricted. The surface erosion is moderate to high with increased erosion in non-vegetated areas with sediments accumulating in low lying regions. The deeper strata are mainly sandy layers, with intermittent shales and coal beds of thickness ~0.2 m to 5 m (Fisher, 1963) (Fig. 9, Table 2).

This area was the site of lignite coal mining that flourished briefly in the early to mid 20th century. Similar to the field site at Malakoff, a detailed history of mining operations that took place at Bastrop in the early 1900's has been difficult to ascertain, which suggests application of a geophysical technique to help identify hidden voids and potential subsidence hazards. Geophysical imaging can reduce the safety and property risk faced by residents of this area. Surficial erosion is distinctly visible in the top soil horizon, in association with small gullies and sand accumulations. There are no other distinct, visible subsidence features on this property in contrast to the numerous Malakoff study area sinkholes. There exists at Bastrop a large kidney-shaped depression or tank with an approximate depth of ~10 m on the property, which seasonally fills with water (Fig. 10). The sides and the base of this feature are smooth, indicating that it is

probably a man made feature and not directly induced by the coal mining subsidence activity.

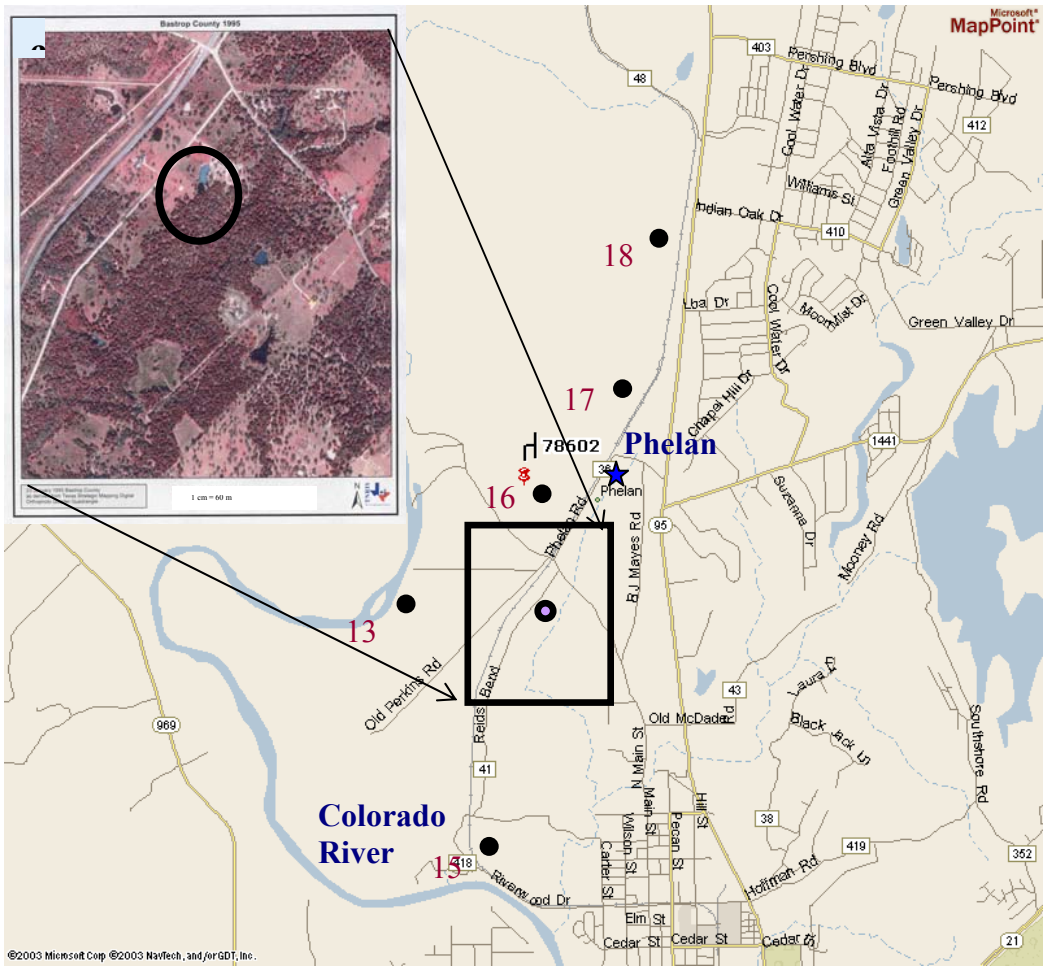

Fig. 9. Location of field site and lignite outcrop at Bastrop. Fisher (1963) identified exposed lignite outcrops at locations numbered in red and represented in table 2. Inset picture: TNRIS Aerial photograph (1995). Map source: Mapquest.com.

Table 2. Exposed lignite section (lignite occurrence) near Bastrop field site

Location	Lignite Occurrence (depth intervals)	
(from fig. 8)	I (m)	II (m)
13	12.6 - 14.3	14.5 - 16.3
15	1.9 - 2.1	4.9 - 5.7
16	3.7 - 5.4	
18	2.1 - 2.2	5.3 - 5.9
19	2.5 - 2.8	8.9 - 11.9

Source: Fisher 1963

Fig. 10. Surficial features (tank) at Bastrop field site. Mr. Carl Pierce in the bean shaped empty/dry tank at Bastrop, Texas. This tank is also seen in the historical aerial photograph from the 1950's with minor visual differences in shape. (Picture taken by Neelambari Save)

GROUND PENETRATING RADAR

Theory of Ground Penetrating Radar (GPR)

The GPR transmitter antenna emits a narrow pulse of several ~ns duration and consequently has a broad frequency spectrum. The dipolar antennae used in this experiment have two octave bandwidths, which means the transmitted frequencies vary between one half and two times the dominant frequency (Conyers and Goodman, 1997). For example, antennae with a dominant frequency of 50 MHz will transmit most efficiently within a range of frequencies between 25 MHz to 100 MHz. The spatial resolution depends on pulse duration and hence bandwidth. Resolution can be improved by increasing the bandwidth and center frequency simultaneously. The depth of investigation varies depending upon material properties and the frequency. Detection of subsurface features depends upon the existence of contrasts in electrical and magnetic properties, and the geometric relationship/orientation of the transmitter and receiver antennae.

When electromagnetic waves from GPR are incident on an interface in which the electromagnetic properties exhibit contrast in the product, part of the energy is reflected back and the remainder is transmitted into the subsurface (Beres and Haeni, 1991). Relative permittivity ε_r, the property of a material which measures its ability to store electric charge when an electric field is applied, is defined as

$$\varepsilon_r = \frac{\varepsilon}{\varepsilon_0} \qquad (1)$$

where ε is the permittivity of the material and ε_0 is the dielectric permittivity of free space.

The amount of reflected energy depends upon the reflection coefficient *R* of the interface which in turn is dependent upon the permittivity. The reflection coefficient is defined by:

$$R = \frac{(V_2 - V_1)}{(V_2 + V_1)} \qquad (2)$$

where V_i is the electromagnetic velocity in medium *i*, for *i* = 1, 2.

The velocity of electromagnetic waves is given by

$$V = \frac{c}{\sqrt{\varepsilon_r}\sqrt{\mu_r}}, \qquad (3)$$

where the speed of light in vacuum is represented by $c = 1/\sqrt{\varepsilon_0}\sqrt{\mu_0}$ = 3 x 10^8 m/s and relative magnetic permeability is represented by μ_r, which in non-magnetic geologic media is μ_r = 1 and is represented as μ_0 in free space. In the case of magnetic geologic media, such as those containing the permeability μ_r > 1, and the electromagnetic wave velocity decreases accordingly (Van Dam, 2002).

Assuming a non-magnetic media, μ_r = 1,

$$V = \frac{C}{\sqrt{\varepsilon_r}} = \frac{1}{\sqrt{\varepsilon_r}\sqrt{\varepsilon_0}\sqrt{\mu_0}} \qquad (4)$$

so that,

$$R = \frac{\sqrt{\varepsilon_1} - \sqrt{\varepsilon_2}}{\sqrt{\varepsilon_1} + \sqrt{\varepsilon_2}} \quad (5)$$

where ϵ_1 and ϵ_2 are the relative permittivities of the two media. The material properties that control the attenuation of electromagnetic waves are permittivity and conductivity. Attenuation (dB/m) is expressed as

$$\alpha = \frac{1.693 \times 10^3 \sigma}{\sqrt{\varepsilon_r}} \quad (6)$$

where σ is the electrical conductivity; defined as the ability of a material to support the long-term flow of an electric current. Table 3 shows the relative permittivity and conductivity of media which are representative of near-surface materials at the Malakoff and Bastrop field sites.

The relative permittivity increases with increasing moisture content. Table 3 indicates that ε_r for water is 81 (maximum possible value), which increases the bulk permittivity of the material through which the electromagnetic waves propagate. Thus moisture can slow the propagation speed significantly in unconsolidated material (Church and Webb, 1986) because of the large water holding capacity in the pore space.

Table 3. Permittivity and conductivity values for various materials (Source: Davis and Annan, 1989)

Material	Permittivity (ϵ)	Conductivity (σ)
Water	81	0.01 - 0.5
Dry Sand	3 - 5	0.01
Shale	5 - 15	1 – 100
Coal	3.5	-

Data Acquisition Technique

Over a period of time, underground rooms and other void features created during removal of the lignite can collapse due to the overlying overburden pressure. If this happens, the void space is filled with disturbed soil and often a surficial feature in the form of a sinkhole is created. The voids/tunnels connecting various rooms also fill with the overlying sediment and sediments that wash in through the mine shafts. The resulting variability in the soil type filling the void/tunnel structure and its contrast with the host sedimentary material could possibly be detected with a GPR survey.

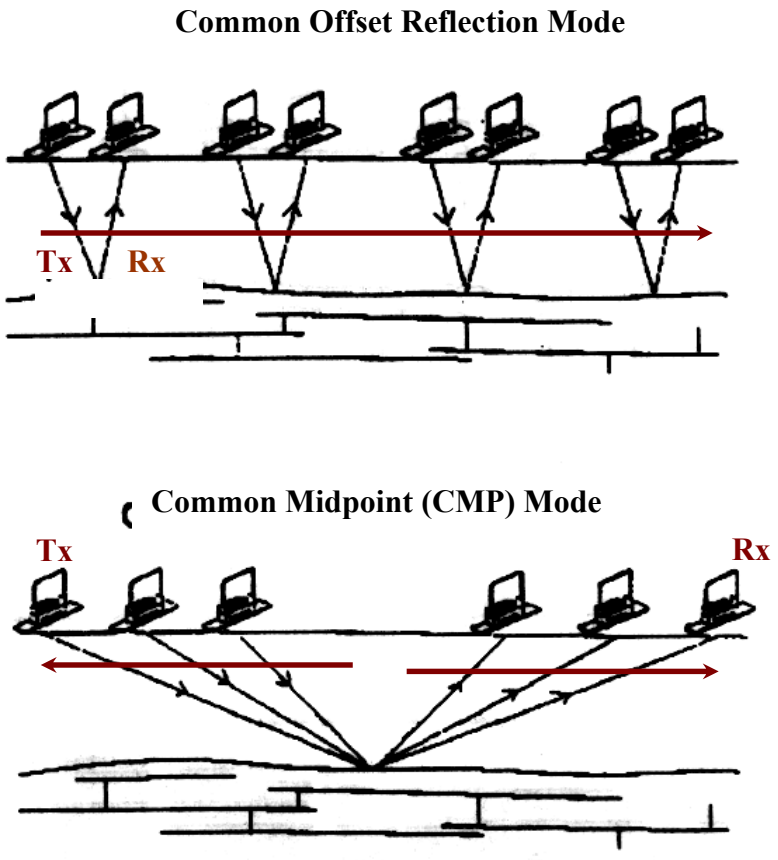

Fig. 11. GPR survey techniques: reflection (common offset) and CMP. Arrows indicate relative movements of transmitter (Tx) & receiver (Rx). (Source: Sensors & Software Inc)

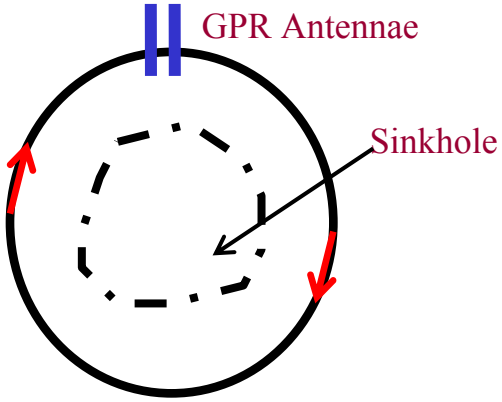

Fig. 12. Sketch of azimuthal survey setup around a sinkhole.

The Sensor & Software Pulse EKKO 100 GPR equipment consists of two antennae: transmitter (Tx) and receiver (Rx); plus a console, fiber optic cables connecting the antennae to the console, and computer to record the data. Two data acquisition strategies commonly used in GPR surveying are reflection (common offset) and common midpoint (CMP) (see Fig. 11). In reflection mode there is a fixed offset between Tx and Rx, which are moved along the survey line at a fixed step size. In the CMP mode, the Tx and Rx are separated from one another in constant increments, but their midpoint is fixed. The information acquired in CMP mode is often used to identify the velocity of the electromagnetic waves. These data acquisition modes are well known in reflection seismology.

An azimuthal pattern of data acquisition is also possible depending upon its feasibility with respect to environmental or man-made obstructions like trees, house,

fence, utility poles etc. In an azimuthal survey (Fig. 12), data are collected at a constant radius along the circumference of the sinkhole. Azimuthal surveys are designed to identify tunnels emanating from the sinkhole thus providing critical risk assessment information regarding connectivity between existing sinkholes. In the absence of a subsurface connection, radar reflections from the edge of the sinkhole should be azimuthally symmetric and in such cases would appear as a consistent feature in the radargram. At the location of an anomaly caused by a subsurface target, such as a tunnel, the azimuthal symmetry of the radargram is broken.

A common midpoint survey (CMP) performed at the field site indicates that the EM wave velocity is 0.1 (± 0.05) m/ns at Malakoff and is 0.1 (± 0.01) m/ns at Bastrop. This velocity (GPR Win_EKKOV10 Manual) is typical for the sandy, shaley lithology seen at Malakoff and Bastrop.

Using the velocity V of the subsurface obtained from CMP mode, and the two way travel time τ of the electromagnetic waves to reflect a particular anomaly, or point on the survey, the depth d can be calculated as,

$$d = \frac{V\tau}{2} \qquad (7)$$

Malakoff: GPR Survey Results and Observation during Reclamation

The subsidence and mine shaft openings at Malakoff studied using GPR are highlighted in Fig. 13.

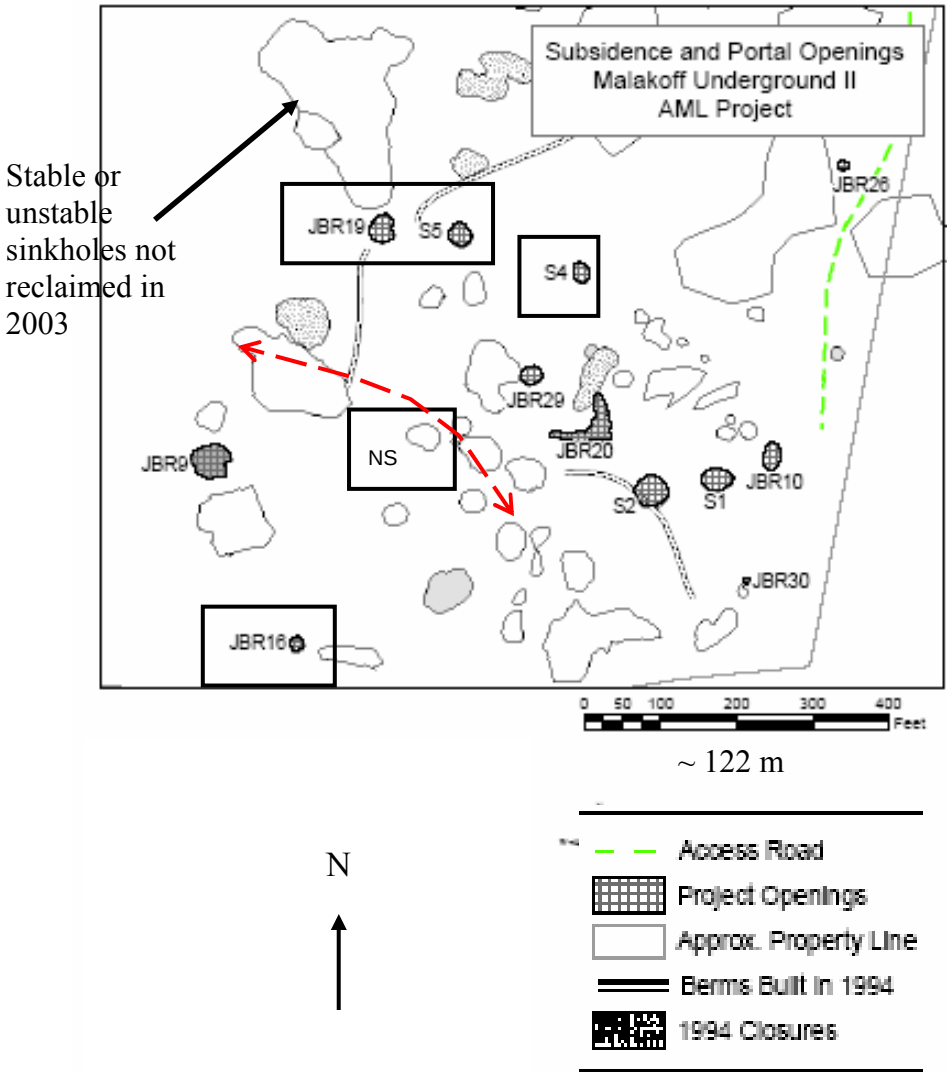

Fig. 13. Sinkholes surveyed using GPR at Malakoff. Red dashed lines indicate some of the trends in sinkhole occurrence. Sinkholes surveyed are boxed. This figure is modified from the RRC document entitled "Malakoff Underground II AML Project invitation for bids".

GPR data were gathered on nine parallel common offset survey lines between sinkholes S-4 and S-5 were gathered. This data set was collected to identify a potential subsurface link between S-4 and S-5. To further test this possibility azimuthal survey around sinkholes S-4 and S-5 were performed. If there is a tunnel connecting sinkhole S-4 and S-5, an anomaly should appear in both the azimuthal surveys and the 9 survey lines. That is, there might be a GPR anomaly heading from sinkhole S-4 toward S-5. Such a connection, if apparent in the azimuthal radargram should also be visible in the 9 survey lines which cross the line joining two sinkholes. Of all the sinkholes that were surveyed, S-4, S-5, JBR-19 and JBR-16 are high priority sinkholes characterized by the team from RRC. In addition to the nine survey lines and sinkholes S-4 and S-5, JBR-19 was also azimuthally surveyed before reclamation in July 2003. JBR-16 was surveyed during the reclamation at Malakoff. Sinkhole NS lines up with adjacent sinkholes represented by a red dotted line-arrow (Fig. 13). Though this is not a high priority sinkhole and was not reclaimed during the 2003 reclamation work, there exists fresh miniature (1.5 m diameter) sinkhole development between these northwest – southeast trending pre-existing sinkholes, strongly suggesting a subsurface connection. Hence, sinkhole NS, in spite of being a non - priority sinkhole, was surveyed. In Fig. 14, a sketch is provided of the survey set up for GPR linear and azimuthal surveys around sinkhole S-4, S-5, JBR-19 and NS and Table 5 summarize these different azimuthal surveys.

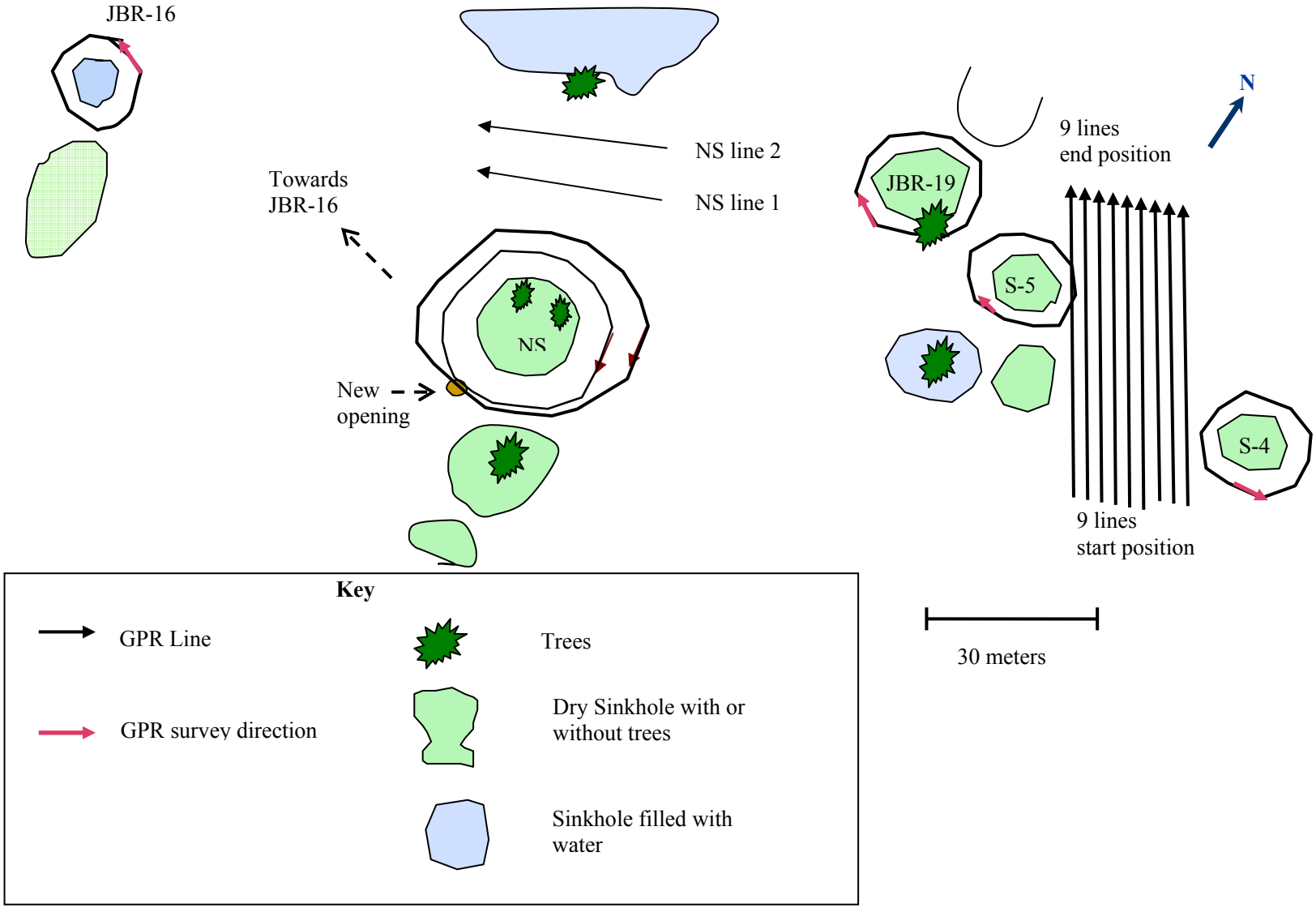

Fig 14. Sketch of GPR survey at Malakoff field site. Orientation of related sinkholes also seen.

Table 4. GPR azimuthal surveys around sinkholes at Malakoff

Sinkhole	Survey Name	Survey Performed	GPR Frequency (MHz)
S-4	S-4	Pre-reclamation	25
S-5	S-5	Pre-reclamation	25
JBR-19	JBR-19	Pre-reclamation	25
JBR-16	JBR-16	During reclamation	100
NS	NS-1	Post-reclamation	50
NS	NS-11	Post-reclamation	50
NS	NS-111	Post-reclamation	100
NS	NS-112	Post-reclamation	100

The findings of the GPR linear common offset survey data and azimuthal survey data at Malakoff are presented in the format:

1. Radargram (image);
2. Results;
3. RRC reclamation results.

Each radargram describes the location of apex of a hyperbola by distance x from the start position of the survey, its depth d, and its two way travel time τ.

Most of the radargrams on the nine survey lines are similar in appearance with hyperbola occurring at a similar depth and location. There is some lateral variability in the anomaly occurrence on the radargrams depending upon the start position of the survey.

25 MHz GPR linear survey at Malakoff between sinkhole S-4 and S-5

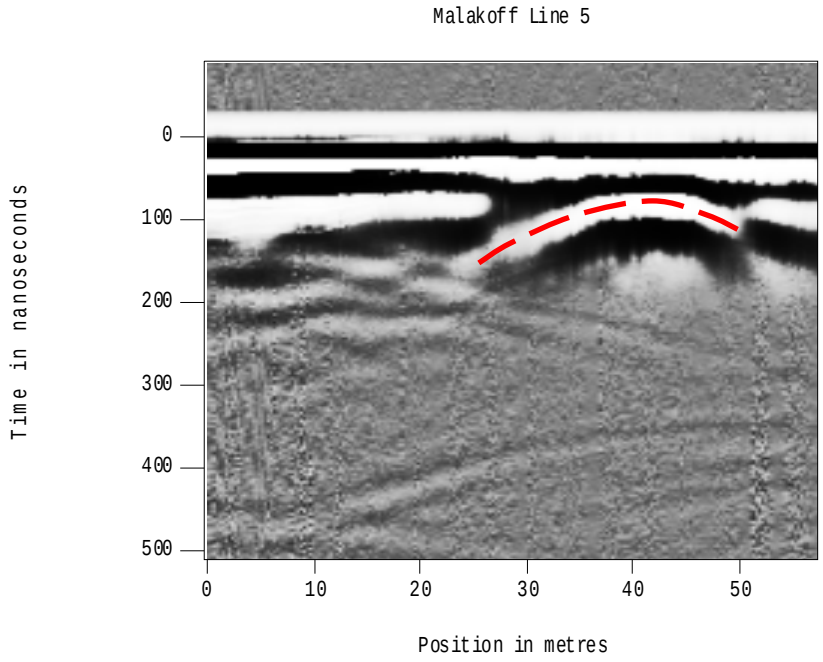

Fig. 15 Radargram of line 5 at Malakoff. 25 MHz GPR linear survey lines located in the area between sinkhole S-4 and S-5.

Results: Hyperbola (marked with red dashed line) observed centered at x ~40 m from the start position and at τ ~80 ns (d ~4 m) in the near surface zone.

Reclamation: The nine lines were not ground-truthed during reclamation and no definitive link between sinkhole S-4 and S-5 using these lines and the azimuthal survey could be identified. Hence, only one (radargram) out of the nine lines has been shown (Fig. 15). Data represented in Figs. 16 – 22 represent azimuthal radargrams around sinkholes at Malakoff.

25 MHz GPR azimuthal survey at Malakoff around sinkhole S-4

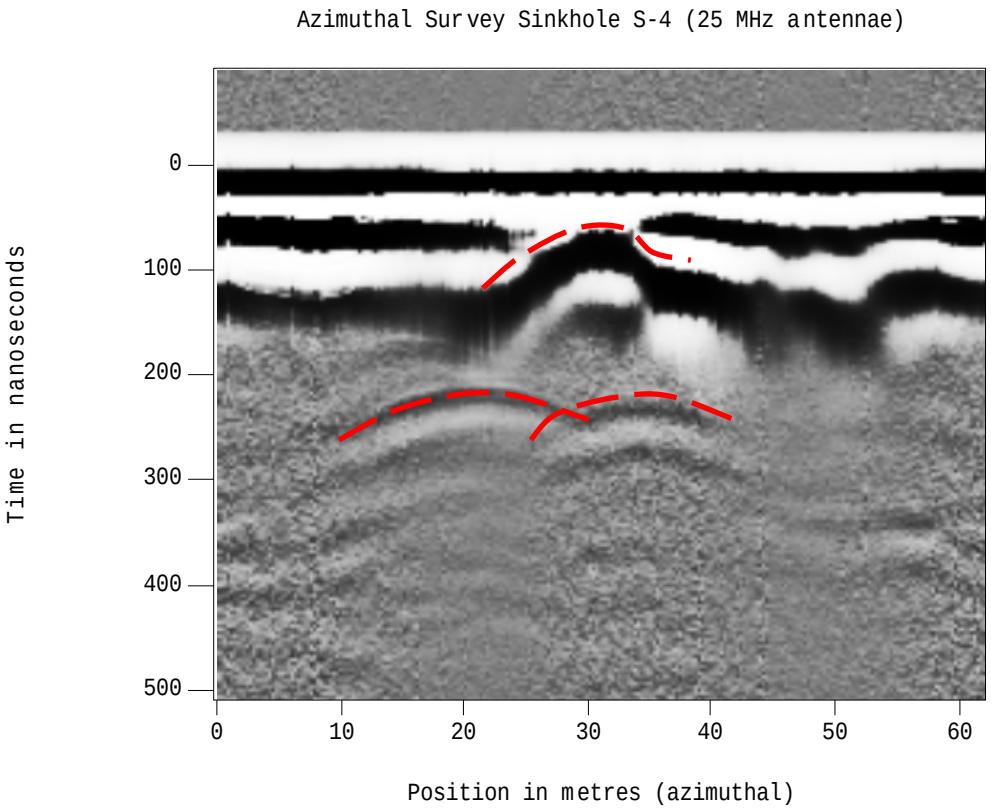

Fig. 16. Radargram for 25 MHz GPR azimuthal survey around sinkhole S-4.

Results: Hyperbolae observed with centers at x ~20 m and x ~35 m from start position with τ ~220 ns and τ ~235 ns (d ~11 m and d ~11.8 m) respectively. The radargram illustrates a washed out image between x ~ 15 – 25 m and x ~ 45 – 55 m. Ambiguous hyperbolae also seen in the near surface zone τ ~80 ns depth (d ~ 4 m).

Reclamation: During reclamation, no tunnels or cavities were found at shallower depths. The backhoe reached a maximum excavation depth of 8 m, and hence the two deeper hyperbolae (seen in Fig. 16) during excavation (d > 8 m) could not be ground truthed.

25 MHz GPR azimuthal survey at Malakoff around sinkhole S-5

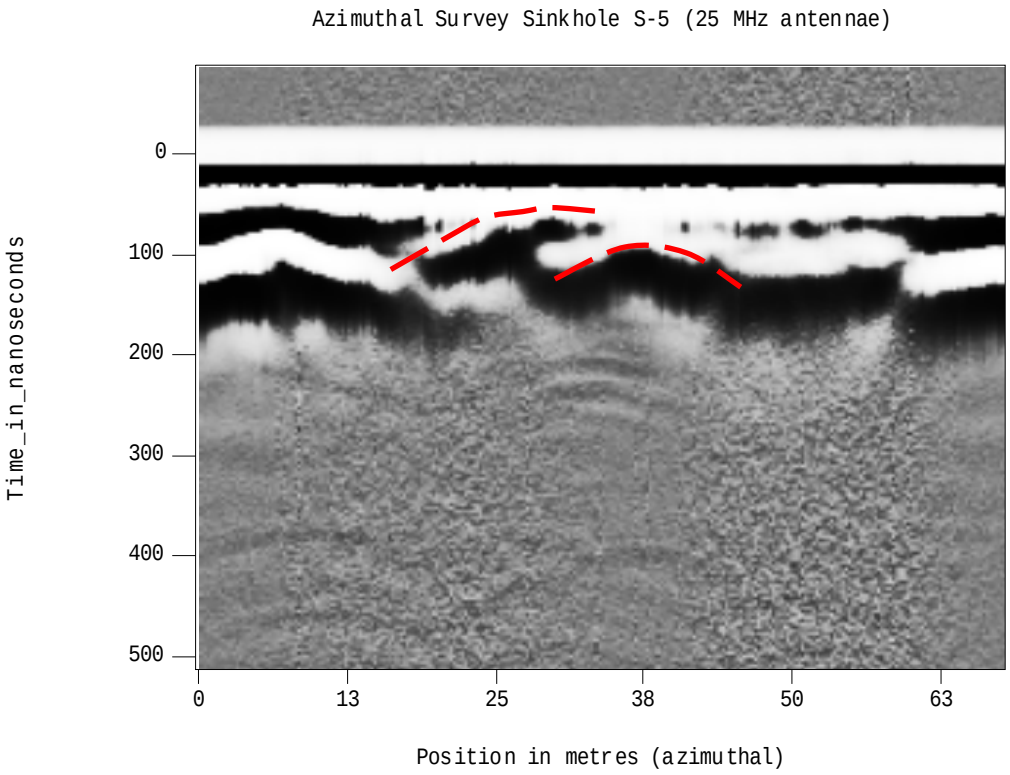

Fig. 17. Radargram for 25 MHz GPR azimuthal survey around sinkhole S-5.

Results: Washed out image at the beginning/end of the azimuthal survey (in Fig. 17). Also seen is a washed out/hazy image with faint hyperbolae at $x \sim 38$ m and $\tau \sim 100$ ns (d ~ 5 m). Prominent disturbed area seen in the near surface zone at $x \sim 25$ m and $\tau \sim 85$ ns (d ~ 5 m).

Reclamations: During reclamation, a tunnel-like feature was observed at depth $d \sim 5.5$ m ($\tau \sim 110$ ns). This tunnel matched the depth of the hyperbola seen in the radargram. The tunnel is possibly heading towards JBR-19 or a sinkhole adjacent to JBR-19.

25 MHz GPR azimuthal survey at Malakoff around sinkhole JBR-19

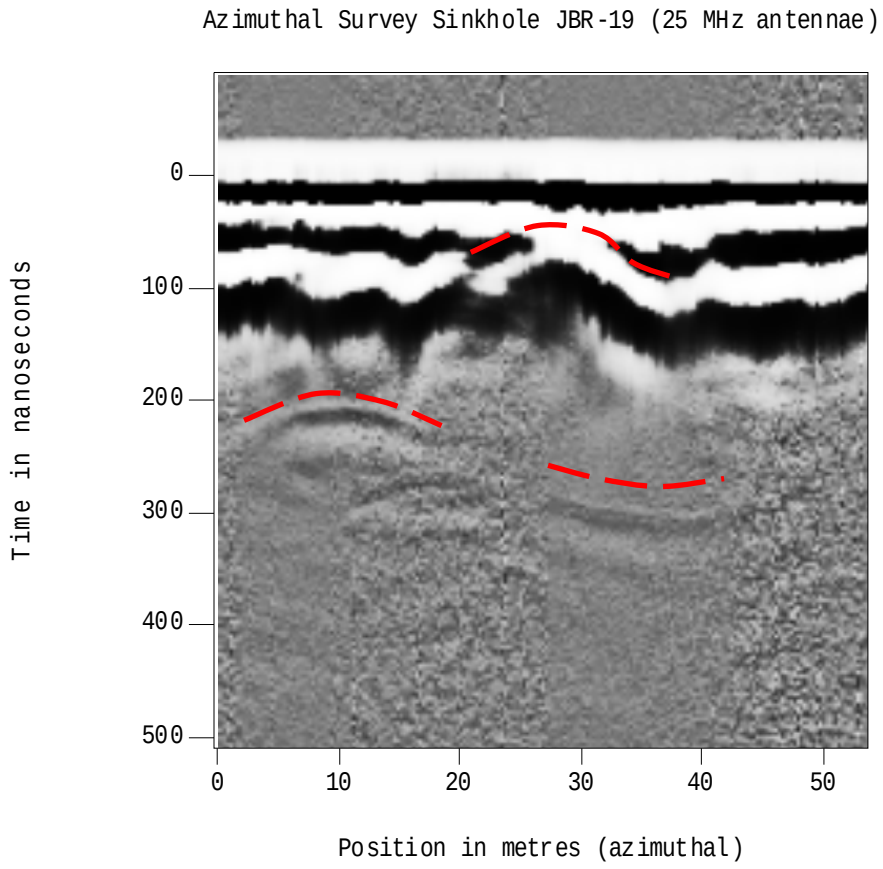

Fig. 18. Radargram for 25 MHz GPR azimuthal survey around sinkhole JBR-19.

Results: Hyperbola observed at $x \sim 10$ m and $\tau \sim 200$ ns ($d \sim 10$ m) and another relatively horizontal feature visible between $x \sim 30$ to 40 m and $\tau \sim 300$ ns ($d \sim 15$ m). In the region (in Fig. 18) below these two features, the radargram has a washed out appearance. Also, an ambiguous hyperbola is seen in the near surface zone ($\tau \sim 50$-100 ns region).

Reclamation: During reclamation, a tunnel-like feature with the x value vaguely corresponding (spatially shifted) to the near surface disturbed zone was seen at $d \sim 4.12$ m. No indication were found of the deeper anomalies observed by GPR. During reclamation, sand lenses with varying iron oxidation and grain size were seen on the walls of the sinkhole. These iron-oxides with $\mu_r > 1$ may have caused the GPR reflections.

Reclamation identified the anomalies which were located in the hazy/disturbed near surface zone for sinkholes S-5 and JBR-19. It was found that most of the causative subsurface targets were much shallower than expected, and hence at the low frequency (25 MHz), a lot of important subsurface information was obscured in the near surface zone. Hence, an azimuthal survey using 100 MHz antennae was performed around sinkhole JBR-16 during the reclamation work in 2003, which provided better resolution of the near surface targets.

100 MHz GPR azimuthal survey at Malakoff around sinkhole JBR-16

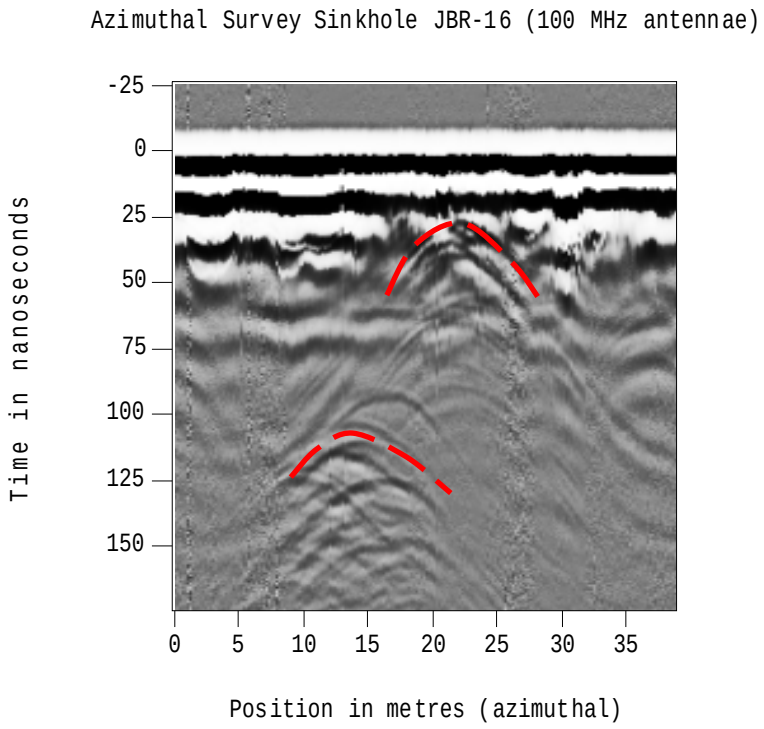

Fig. 19. Radargram for 100 MHz GPR azimuthal survey around sinkhole JBR-16. This dataset was collected during reclamation (after excavation of sinkhole S-4, S-5 and JBR-19).

Results: Hyperbola observed at x ~12 m and τ ~112 ns (d ~ 6.6 m), with multiples, and a bow tie effect below it in Fig. 19. Hyperbola also seen at x ~22 m and τ ~ 25 - 60 ns (d~

1.2 – 3.0 m) followed by multiples and washed out image. Disturbed regions seen in the near surface zone.

Reclamation: Tunnel like feature seen starting at d ~2.74 m with a base at d ~ 4.27 m at x ~22 m. When visually inspected before the reclamation, a surficial depression was observed between JBR-16 and an adjacent sinkhole. During excavation of JBR-16, water started accumulating in the sinkhole and as a result the backhoe was used to dig up to d ~ 6 m and not much information could be obtained at $d > 5$.

Post reclamation, more data were collected around sinkhole NS to try to develop a technique which reduces false alarms and confirms an anomaly by line to line repeatability. Hence, azimuthal surveys were performed around sinkhole NS using 50 MHz and 100 MHz GPR antennae with multiple radii around the circumference of the sinkhole.

50 MHz GPR azimuthal survey at Malakoff around sinkhole NS with 3 m radii

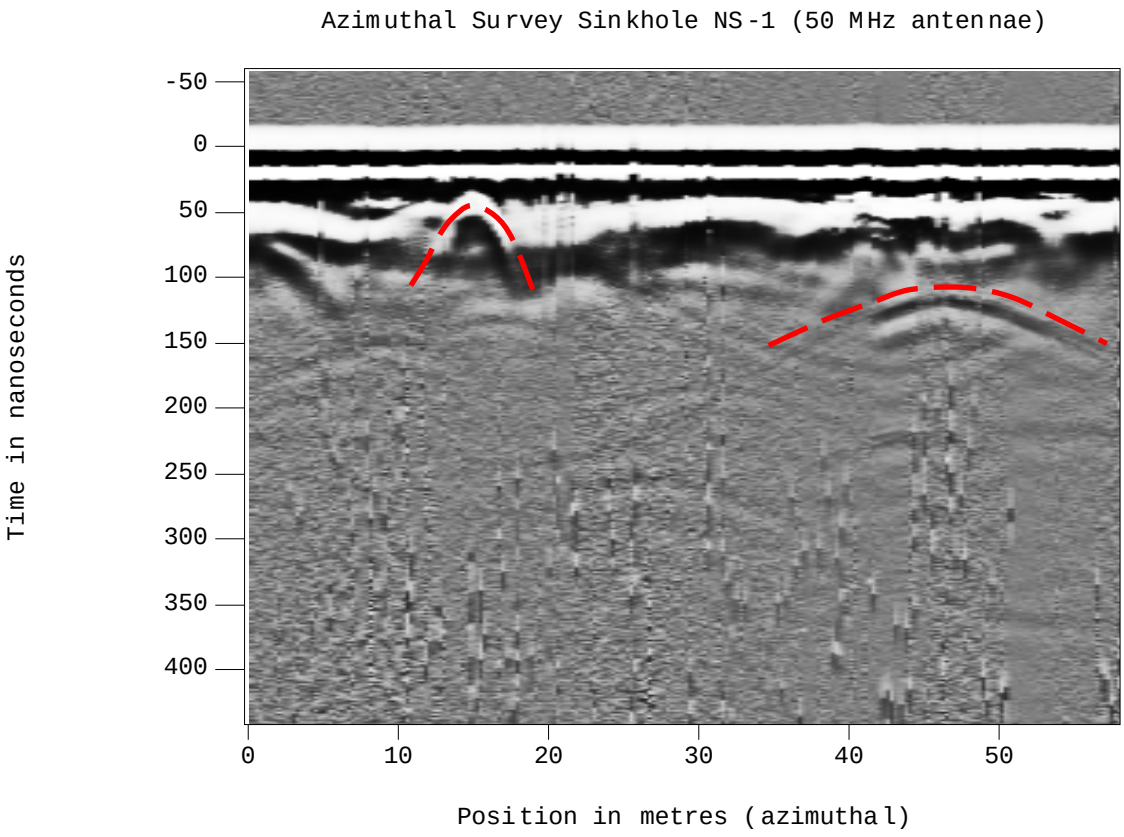

Fig. 20. Radargram NS-1 for 50 MHz GPR azimuthal survey (around sinkhole NS). Survey radius is 3 m greater than the radius of the sinkhole.

Observations: At $x \sim 15$ m the survey passed over a small opening (future possible massive sinkhole opening) creating a small tight hyperbola. Hyperbolae observed on the radargram (in Fig. 20.) at around $x \sim 47$ m and $\tau \sim 100$ ns ($d \sim 5$ m).

Reclamation: Data were collected after the reclamation was performed, and hence no ground truthing for the data.

50 MHz GPR azimuthal survey at Malakoff around sinkhole NS with 5 m radii

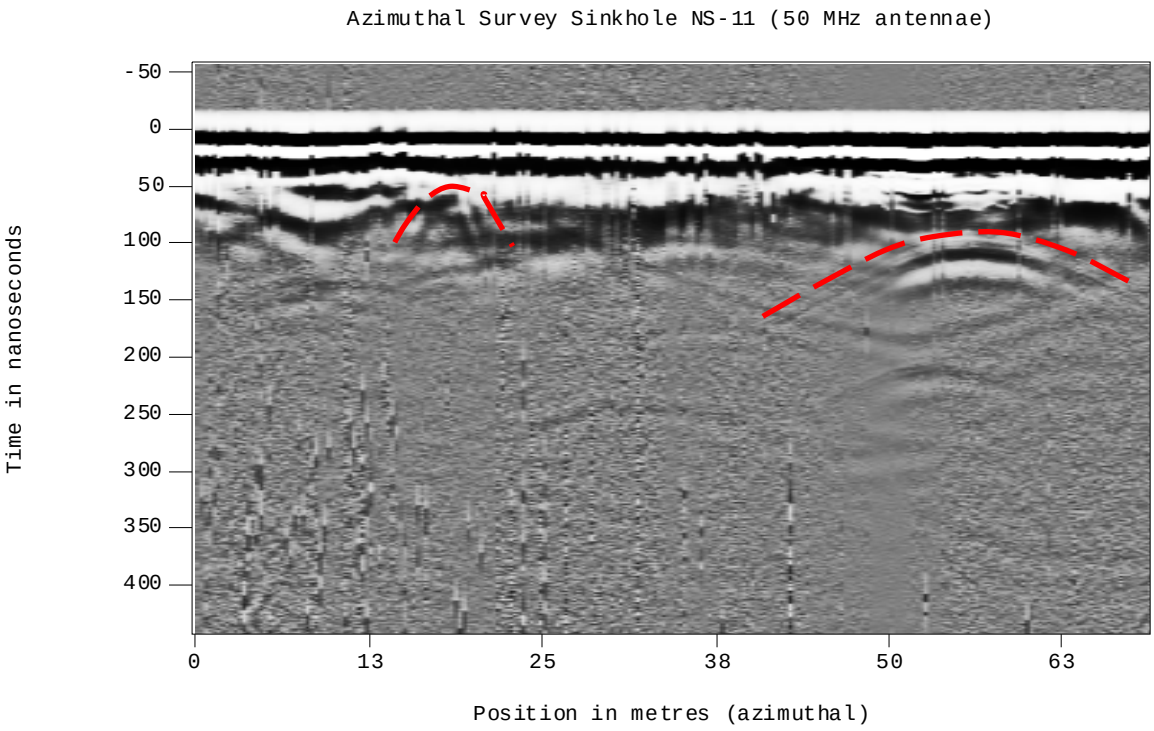

Fig. 21. Radargram NS-11 for 50 MHz GPR azimuthal survey. Radius 5 m greater than the radius of sinkhole NS.

Observation: Major hyperbola seen at around x ~57 m and τ ~ 100 ns (d ~ 5 m). Hazy image detected between 45 m and 55 m in Fig. 21. The sinkhole passed over a small opening at x ~ 19 m creating a small tight hyperbola.

Reclamation: Data were collected after the reclamation was performed.

The 100 MHz antenna was used to collect data along the same azimuthal set up (as in NS-11), but the survey abruptly ended at x ~ 20 m due to technical difficulty (battery drain). Since no strong signals were seen in the azimuthal surveys NS-1 and NS-11 in the first 50 m, a newer dataset was named NS-112 and data was gathered later starting at x ~ 52 m and ending at x ~ 80 m after replacing the battery. This range x ~ 52 - 80 m was chosen because hyperbolae were seen on Line NS-1 and NS-11 in this region.

100 MHz GPR azimuthal survey at Malakoff around sinkhole NS with 5 m radii

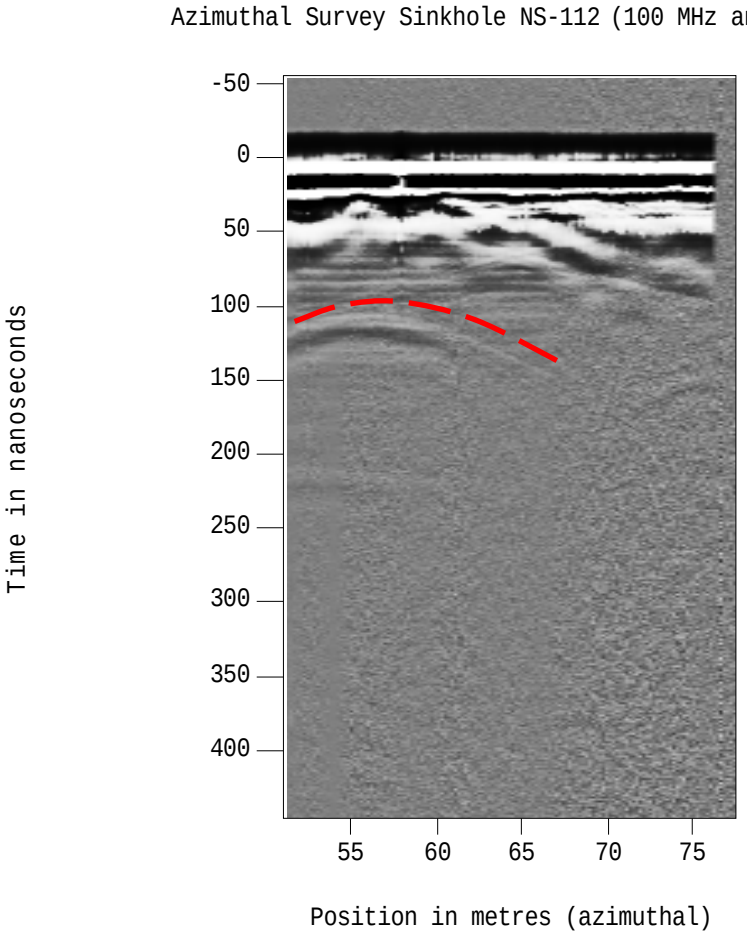

Fig. 22. Radargram NS-112 for 100 MHz GPR azimuthal survey. Radius 5 m greater than the radius of sinkhole NS.

Observation: Hyperbola seen centering at $x \sim 56$ m and $\tau \sim 110$ns ($d \sim 5.5$ m). This hyperbola seen in Fig. 22 occurs at the same general location as the one seen at NS-11.

Reclamation: Data were collected post reclamation phase, hence no ground truthing.

50 MHz GPR linear survey at Malakoff 6.7 m from the circumference of sinkhole NS

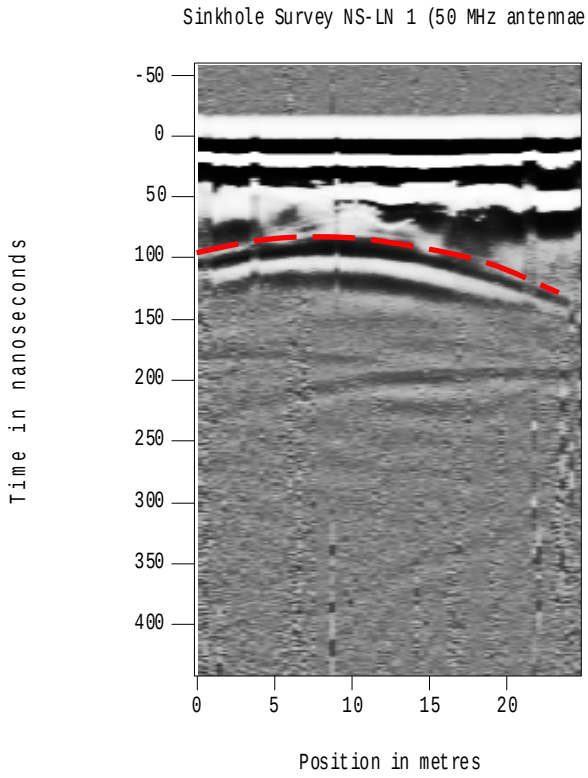

Fig. 23. Radargram NS-LN1 for 50 MHz linear survey (sinkhole NS). The survey set up is set up 6.7 m away from the circumference of the sinkhole NS.

Observations: Hazy image spread out hyperbolae seen centering $x \sim 12$ m and $\tau \sim 100$ ns ($d \sim 5$ m) in Fig 23.

Reclamations: Data were collected post reclamation phase, hence no ground truthing.

50 MHz GPR linear survey at Malakoff 11 m from the circumference of sinkhole NS

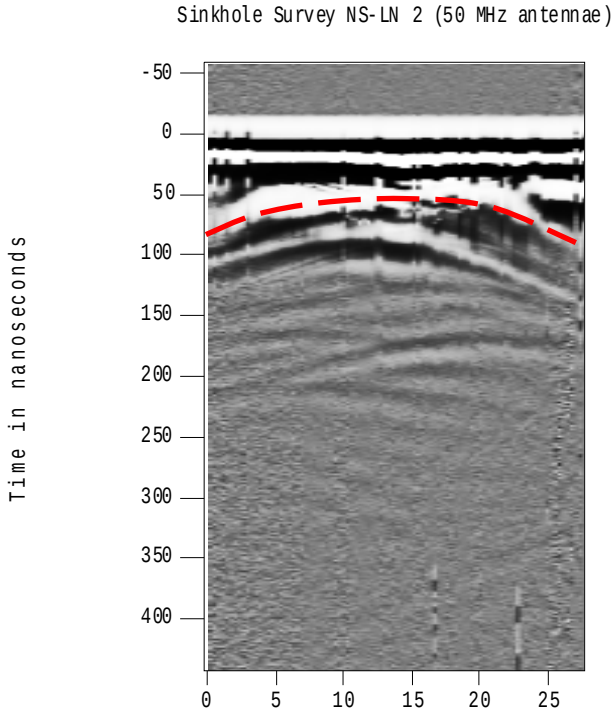

Fig. 24. Radargram NS-LN2 for 50 MHz linear survey (sinkhole NS). The survey set up is set up 11 m away from the circumference of the sinkhole NS.

Observations: Hazy image, spread out hyperbolae seen centering $x \sim 10$ m and $\tau \sim 100$ ns ($d \sim 5$ m) in Fig. 24.

Reclamations: Data was collected post reclamation phase.

A map has been created showing the different anomalies detected and identified during ground truthing in the discussion section of the thesis. The next section describes the survey at Bastrop. The data is reported in the following format:

1. Radargram 2. Observation

Bastrop Area 1: GPR Survey Results

The survey at Bastrop Area 1field site is surrounded by a lot of man-made and natural structures as seen in Fig. 25 thus increasing the noise level in the data set

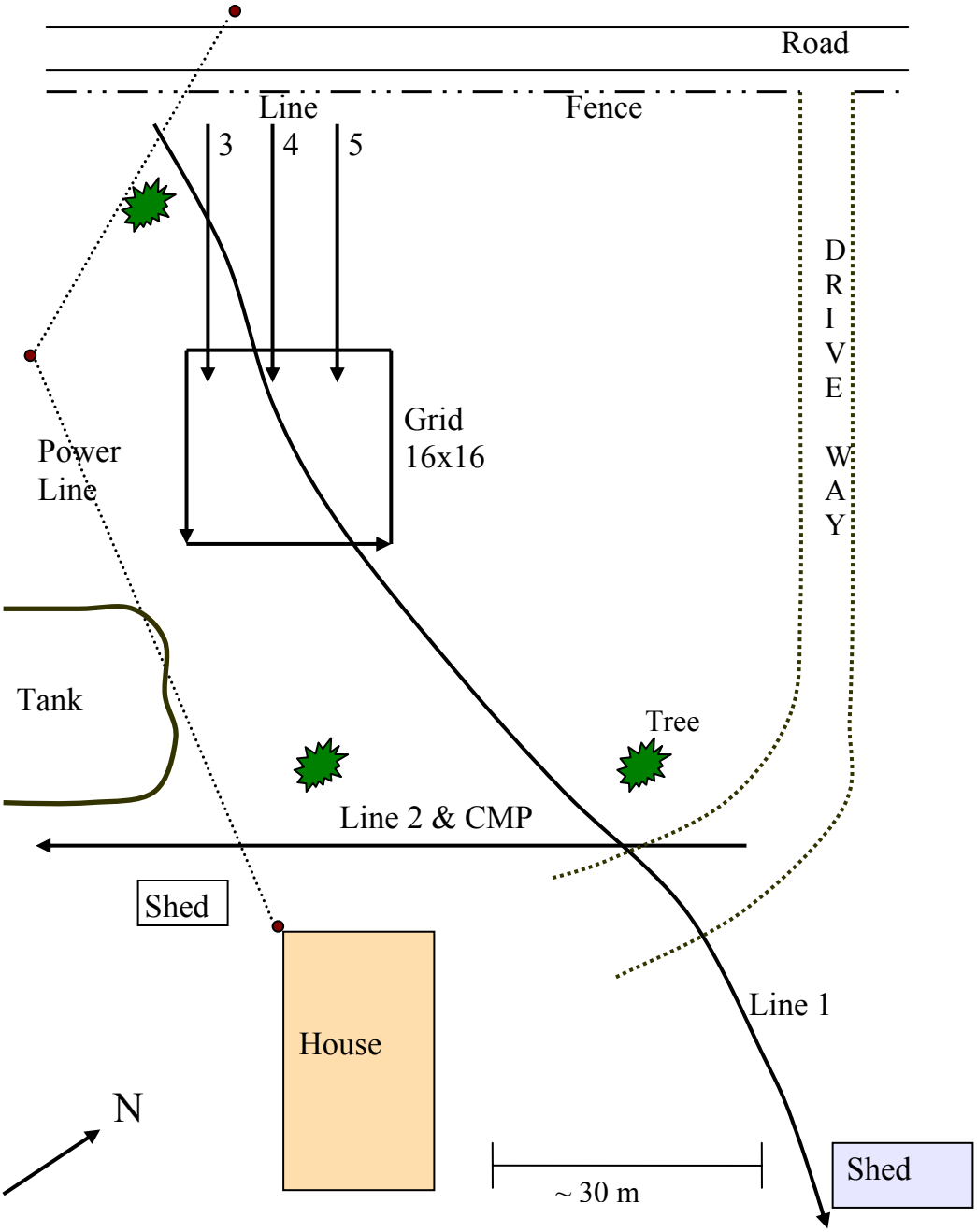

Fig 25. GPR survey set up for Bastrop Area 1

25 MHz GPR linear survey at Bastrop Area 1 – Line 1

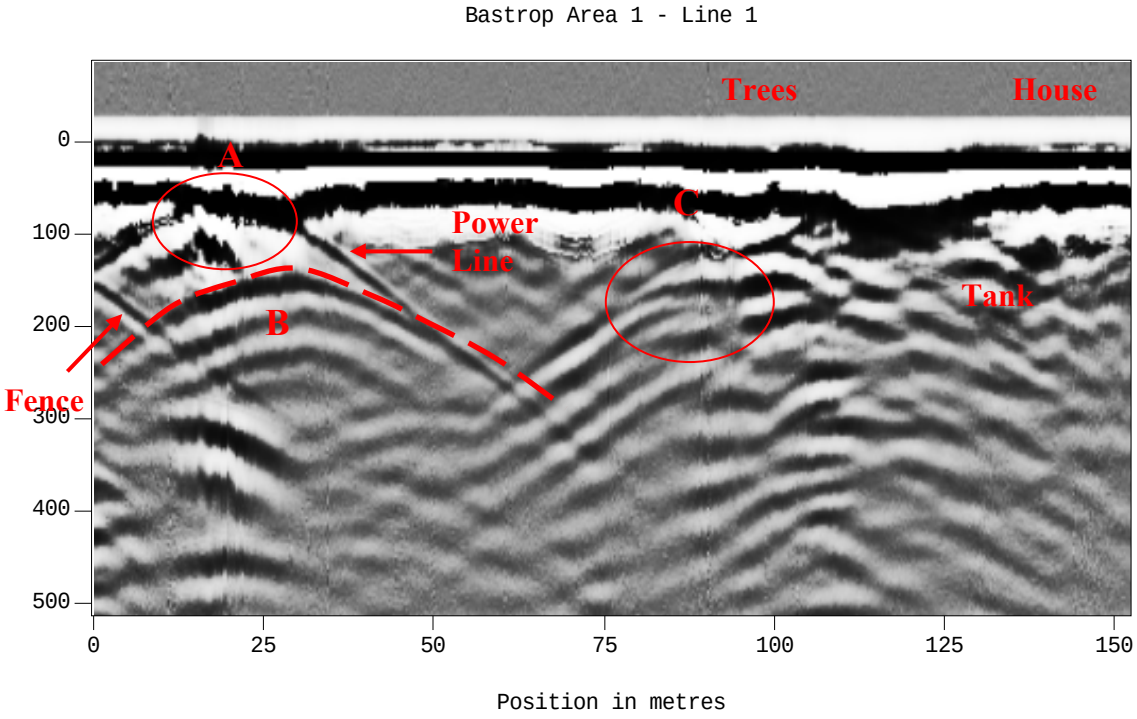

Fig. 26. Radargram for 25 MHz GPR linear survey on line 1 at Bastrop (Area 1). Reflection from several man-made and natural objects is observed.

Observation: Reflection from the surficial features like the fence, power line, tress, and house are seen in the radargram in Fig. 26. A disturbed hyperbola (A) is seen at $x \sim 20$ m and $\tau \sim 80$ ns ($d \sim 4$ m) depth (interfering with the reflection of the power line). Hyperbola (B) at $x \sim 30$ m and another hyperbola (C) at $x \sim 85$ m and $\tau \sim 180$ ns ($d \sim 9$ m) depth seen in the radargram. The latter hyperbola signal is dominated by strong reflections, possibly from trees between which the survey line passes.

25 MHz GPR linear survey at Bastrop Area 1 – Line 2

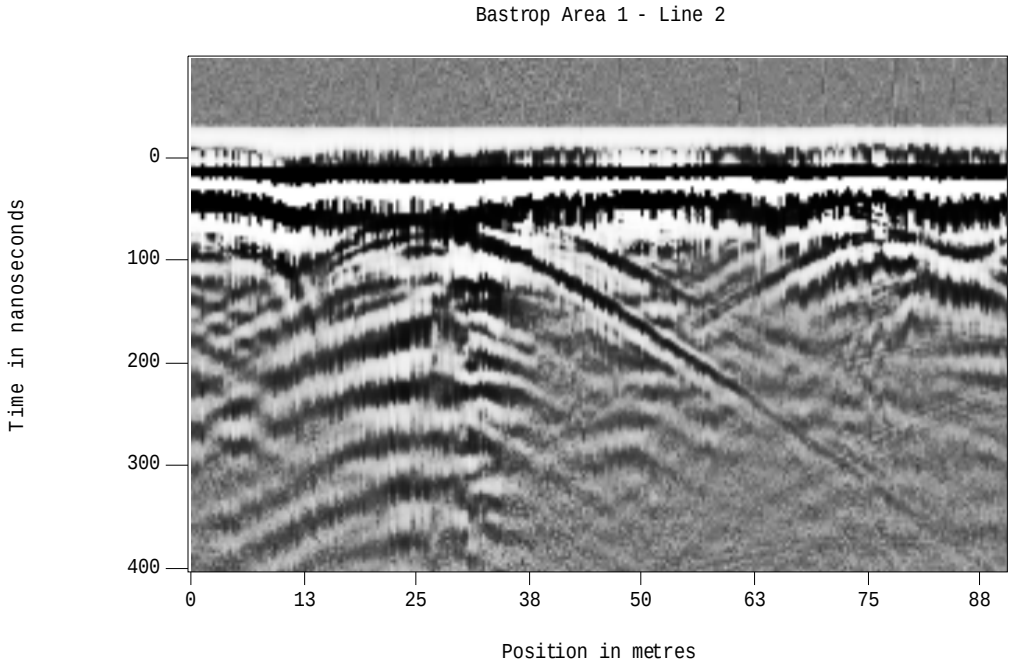

Fig. 27. Radargram for 25 MHz GPR linear survey on line 2 at Bastrop (Area 1).

Results: Line 2 is adjacent to the house, a couple of trees and a metallic shed containing heavy farm equipment. The hyperbolae seen in the radargram (Fig. 27) occurred when the GPR unit passed by these objects, essentially meaning that it is caused by cultural noise. At Malakoff, there occurred hazy region or disturbed region below a hyperbola where a possible tunnel was identified. Line 2 lacks any such prominent features.

25 MHz GPR linear survey at Bastrop Area 1 – Line 3, 4 and 5

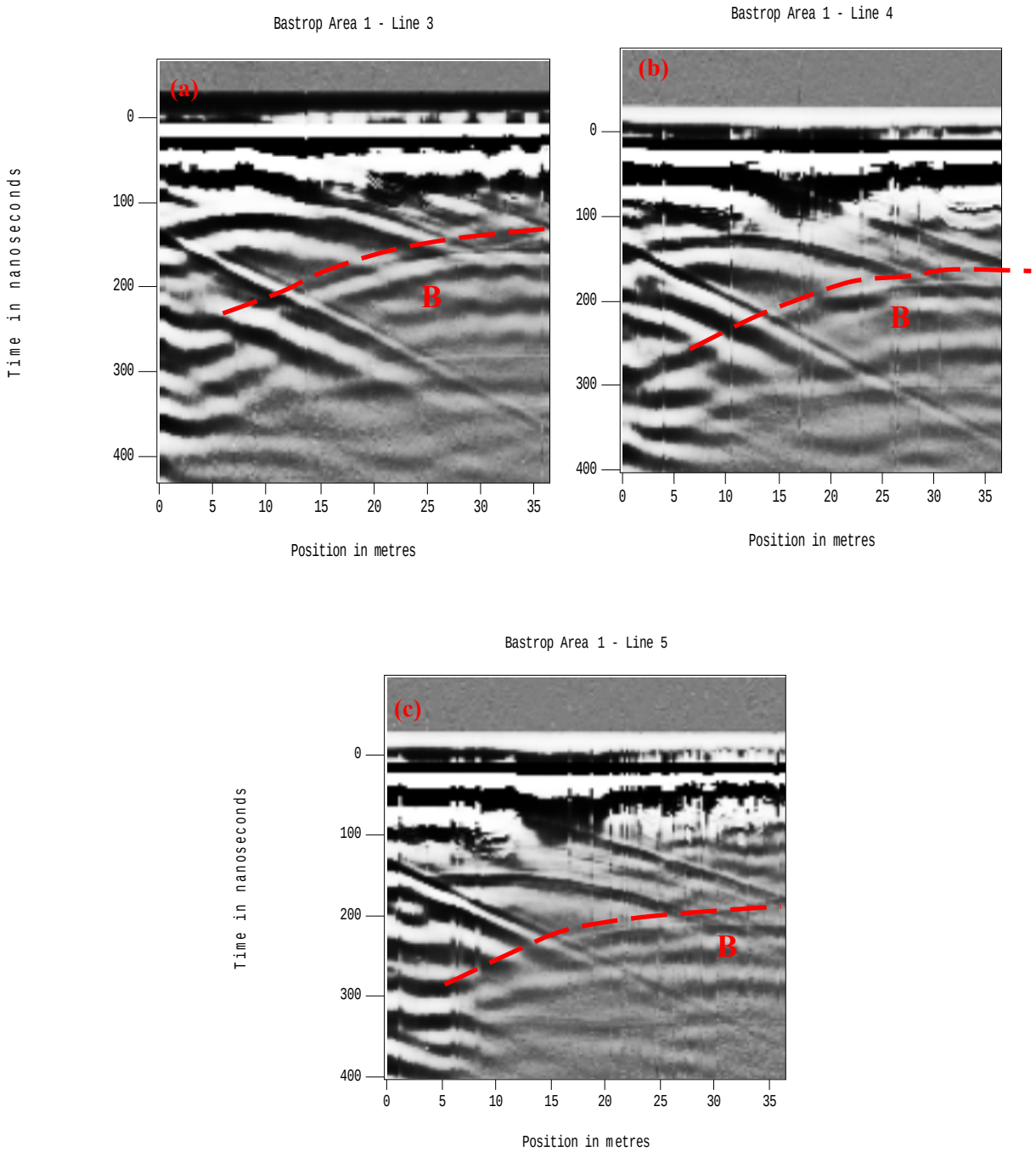

Fig. 28. Radargrams for 25 MHz GPR linear survey on line **(a)** 3, **(b)** 4, and **(c)** 5 at Bastrop (Area 1).

Results: Bastrop Area 1 – Lines 3, 4 and 5 are parallel to each other with a separation of 4 m between each survey line. All the three radargrams (Fig. 28) are similar with hyperbolae B present and disturbances at relatively the same distance from the start position and at approximately the same depth. These radargrams match with the first 36 m of data for line 1 (Fig. 26).

A 3-D grid was surveyed, but the grid was too small with not much of an overlap with the other data that was collected. The image was not very informative and needed a higher resolution and area coverage.

Discussion

The data collected at Malakoff were ground-truthed by RRC Texas in June 2003 during the reclamation process. The linear survey lines were not ground truthed, only sinkhole S-4, S-5, JBR-16 and JBR-19 along with some other sinkholes were reclaimed. Sinkhole S-4, S-5 and JBR-19 azimuthal surveys were performed before the reclamation process using the 25 MHz antenna. A tunnel-like feature (Fig. 29) was observed in S-5 during the reclamation whose depth matched with the GPR data depth prediction, though there appeared to be a slight shift in the lateral position.

Fig. 29. A tunnel found at Malakoff in sinkhole S-5 during reclamation. The tunnel was filled with oxidized sand

The anomalies predicted at S-4 were very deep, beyond the reach of the backhoe, and hence these anomalies could not be verified. A tunnel was located during reclamation at JBR-19 which probably appeared in the ambiguous near surface zone on the GPR data. Occurrence of anomalies in the near surface zone, leads to ambiguity about their existence and hence a better survey design or approach is required. Ground truthing suggested that the tunnels were much shallower than expected. Hence, the 25 MHz antenna was probing too deep and the most informative signal was being ignored since it manifested itself in the near surface zone. As a result, 100 MHz antenna was used for the survey of JBR-16 during the reclamation. The anomaly detected at this sinkhole matched with a tunnel like feature observed during reclamation. Also, during the reclamation it was noticed that there were abundant clay/sand lenses with great variation in its color (oxidation of the Fe rich minerals) and grain size (Fig. 30).

Fig. 30. Color variation in soil observed during reclamation of sinkhole JBR-19. (Source: RRC, Tx)

Some of the (broad) hyperbolae could have been reflection from these lenses. Variation in the physical properties can also lead to variation in the water holding capacity of the various stratigraphic layers or lenses, resulting in greater attenuation of the EM signal in some regions and a washed out hazy image in the radargram. According to Crowell, (2001), when a mine roof collapses, there exists incomplete compaction due to crumbling and falling of the roof. This could possibly result in a hazy radar signature due to small scale reflection and scattering of the electromagnetic waves.

The GPR data and the ground-truthing indicated a need for a technique to verify anomalies using multiple frequency antennae and multiple surveys around a sinkhole. Hence, a multiple radii survey was performed using 50 and 100 MHz antennae around sinkhole NS. After noting a consistent anomaly (relatively same location on survey and same depth underground) on multiple azimuthal surveys around sinkhole NS, data were gathered on 2 linear lines moving farther away from the sinkhole. This was done to verify if the anomaly continued laterally in space. Hyperbolae were observed on all the surveys (Fig. 20 to Fig. 24: Survey NS-1, NS-11, NS-112, NS-LN1, NS-LN2) that were performed around sinkhole NS indicating that multiple radii and frequency can be used to identify and confirm an anomaly. Had this approach been used in the earlier surveys (S-4, S-5 and JBR-19), the anomalies that were not detected with GPR may have been identified. The results of the GPR survey at Malakoff for sinkhole S-4, S-5, JBR-16, JBR-19 and NS are shown in Fig. 31. The identification of tunnel-like features for reclaimed sinkhole or un-reclaimed sinkhole have been color coded in order to identify the success rate verses the false alarm for the GPR data.

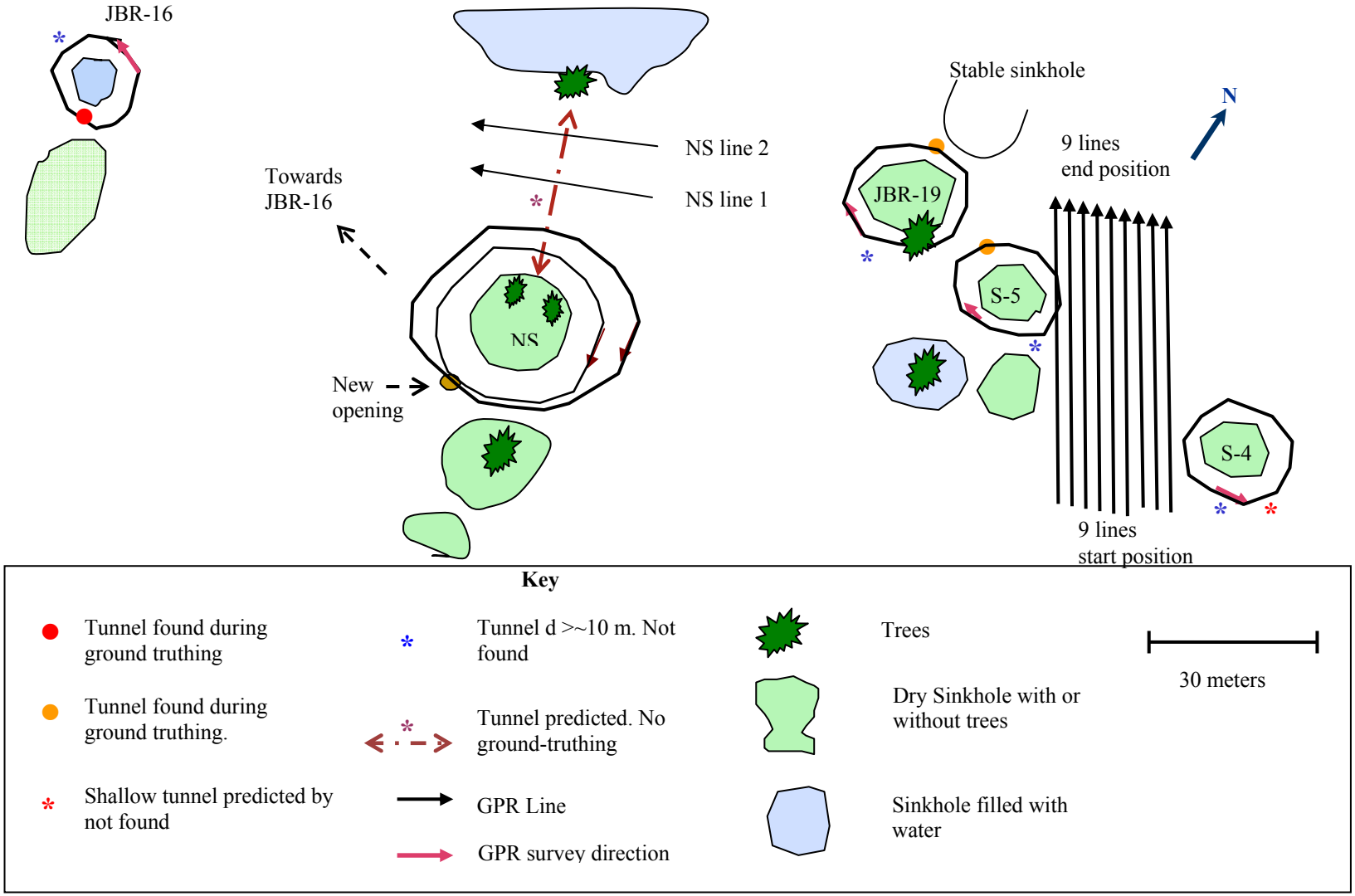

Fig 31. Sketch of GPR survey at Malakoff with identified anomalies and results of ground truthing.

Unlike Malakoff, no ground-truthing or reclamation has been performed at Bastrop Area 1 (until September 2004). Bastrop Area 1 also lacked any physical evidence of fresh collapse or sinkhole openings at the field site. There was however sinkholes like the ones at Malakoff a mile west of the Bastrop field site. There was abundant surficial erosion, in which sand is transported and deposited in lower elevated areas. The erosion appears to be a result of lack of vegetation at the field site. The owner also complained about small holes opening up and swallowing water after rainfalls. Hyperbolae on the GPR lines are in good spatial alignment on lines 1, 3, 4 and 5, but there are no supporting data (ground-truthing, sinkholes, collapses etc) available. An alternative geophysical method is required to do that. Hence, data was collected using the Wenner Resistivity method at the field site (described in section "Supporting Data for Bastrop Field Site"). GPR survey was also performed in an area adjacent to the main survey area at Bastrop. The new site was called survey Area 2 and the data for this survey is represented in Appendix A.

RECLAMATION AT MALAKOFF

Since reclamation provides ground-truthing, it is important to have a basic understanding of the procedure. Soil is dug out from sinkholes using a backhoe (Fig. 32 (a)), which can reach a maximum depth of around 8 m. The soil is then piled beside the excavated sinkhole. Any non-stable collapsed part of the sinkhole is stabilized and then filled up. In this case 300 truck load of fill material (clayey loam) from Trinidad, Texas was required to seal the sinkholes. The imported soil is used to fill the base of the sinkhole after which the soil dug out of the sinkhole is used to fill the rest of the sinkhole. The backhoe is used to compact the soil (Fig. 32 (b)).

Fig. 32. Reclamation process at Malakoff (July 2003). **(a)** Backhoe used to dig and remove soil from a sinkhole, **(b)** Backhoe thumping the ground to compact the soil while filling the sinkhole

Filling of the sinkholes was followed by re-vegetation of the area to give it a natural look and to reduce surface erosion. The reclamation process of a sinkhole is depicted in Fig. 33. The total cost of the project was approximately $ 46,000 and the reclamation work lasted for about 10 days.

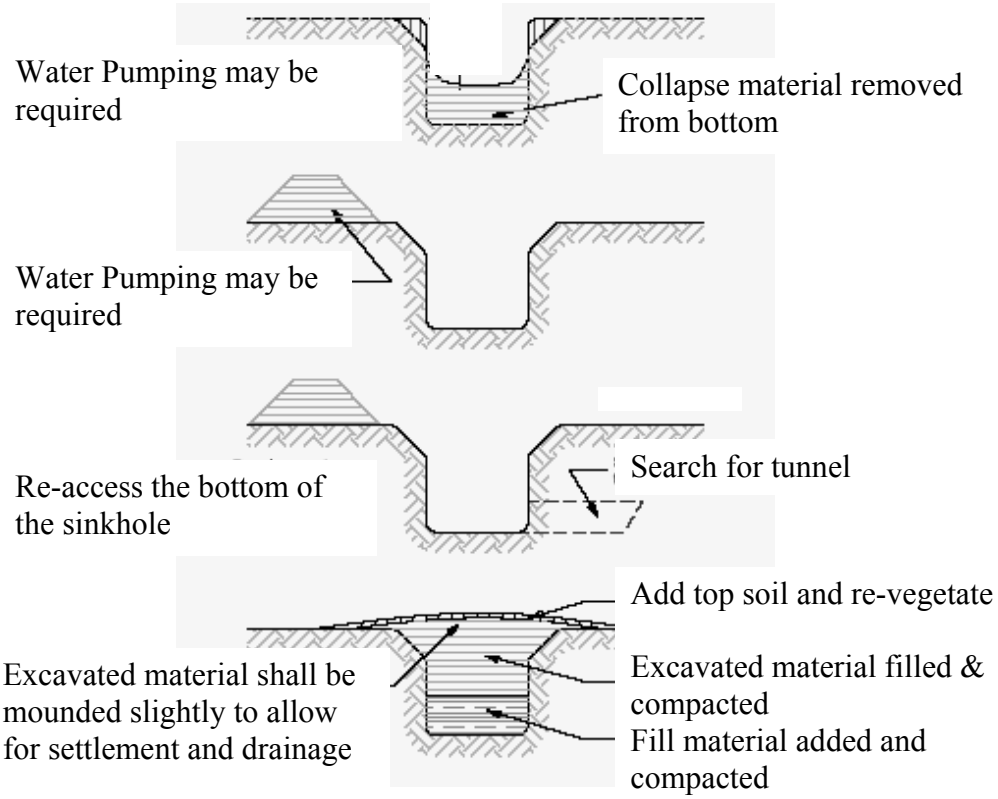

Fig. 33. Typical mine subsidence sinkhole closure sequence (Modified from Railroad Commission of Texas Invitation for Bids for Malakoff Underground II Abandoned Mine Land (AML) site (FY 2003)).

SUPPORTING DATA FOR BASTROP FIELD SITE

Resistivity Theory

Wenner electrode resistivity configuration (Fig. 34) was used along the survey lines setup using Advanced Geosciences, Inc. STING R1™ resistivity equipment. In the Wenner configuration, the two outside electrodes (I_1 and I_2) introduce a current into the ground, and the two inside electrodes (P_1 and P_2) measure the potential difference (V) between them caused by the DC current (Fig. 34).

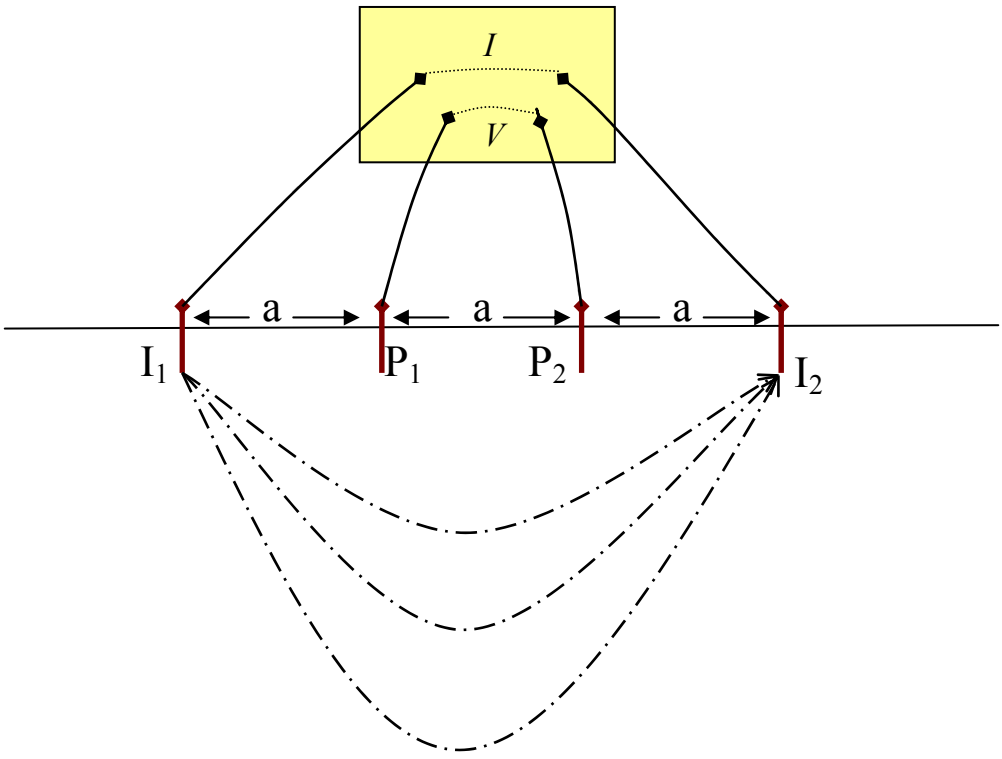

Fig. 34. Wenner resistivity arrangement used at Bastrop.

The property of the electrical resistance of a material is usually expressed in terms of its resistivity (measured in ohm meter (Ωm)) (Sharma, 1997). For a conducting body of length l, area A and resistance R, the resistivity ρ is

$$\rho = \frac{RA}{l}. \tag{8}$$

According to Ohm's law, the potential difference across the conducting body is

$$\Delta V = RI. \tag{9}$$

Hence in case of a homogeneous isotropic earth layer,

$$\frac{\Delta V}{l} = \frac{\rho I}{A} \tag{10}$$

If the conducting layer length (l) tends to zero in Equation 10, then

$$-\Delta V = \rho I \tag{11}$$

If a current I is passed through the ground surface, it will flow radially and spread out uniformly over a hemispherical shell of a surface area of $2\pi r^2$ at a distance r from the current source. Hence, the current density i is

$$i = \frac{I}{2\pi r^2}. \tag{12}$$

Therefore,

$$\frac{-\delta V}{\delta r} = \rho i = \frac{\rho I}{2\pi r^2}; \tag{13}$$

and potential at a distance r is

$$V_r = \frac{\rho I}{2\pi r} + C, \tag{14}$$

where C is a constant of integration

The potential difference between the two potential electrodes (Fig. 34) caused by the current at the source I_1 is

$$\Delta V = \frac{\rho I}{2\pi\left(\frac{1}{I_1P_1} - \frac{1}{I_1P_2}\right)}. \qquad (15)$$

Similarly the potential difference between the two potential electrodes (Fig. 34) at the sink I_2 is

$$\Delta V = -\frac{\rho I}{2\pi\left(\frac{1}{I_2P_1} - \frac{1}{I_2P_2}\right)} \qquad (16)$$

Hence, the total potential difference is

$$\Delta V = -\frac{\rho I}{2\pi\left(\frac{1}{I_1P_1} - \frac{1}{I_1P_2} - \frac{1}{I_2P_1} + \frac{1}{I_2P_2}\right)} \qquad (17)$$

therefore,

$$P = \frac{2\pi\Delta V}{I}\frac{1}{G} \qquad (18)$$

Where G = $\left(\frac{1}{I_1P_1} - \frac{1}{I_1P_2} - \frac{1}{I_2P_1} + \frac{1}{I_2P_2}\right)$ and $\frac{2\pi}{G}$ denotes the "geometric factor" of electrode configuration. Equation 18 is valid under homogeneous conditions; therefore resistivity in an inhomogeneous medium is conceptualized as an apparent

resistivity (ρ_a). In case of Wenner array, the four electrodes are equally spaced ('*a* spacing ') along a straight line, thus reducing the equation for the apparent resistivity to

$$\rho_a = 2\pi a \frac{\Delta V}{I}. \qquad (19)$$

The technique of Wenner resistivity allows geoelectric mapping of the subsurface which measures the spatial variation of earth resistivity within a certain depth range (Bhattacharya and Patra, 1968). The effective depth of penetration varies depending upon factors such as: current source, presence of in homogeneities, resistivity contrast, and degree of electrical anisotropy (Sharma, 1997). However, assuming that the subsurface is homogeneous, the depth of penetration of the Wenner configuration according to Burger (1992) is

$$z = \frac{3a}{2}. \qquad (20)$$

Most of the anomalies seen in the GPR radargrams are less than 10 m in depth. Hence if there exists a possible anomaly caused by a (filled/empty) tunnel, it should be detected due to the resistivity contrast by Wenner technique using an '*a* spacing' of ~7 m.

A Wenner resistivity survey was performed at Area 1 (Fig. 35) along lines1, 2, 3 and 4 with '*a* spacing' of 7 m and a step size of 7 m. To increase the resolution and probability of identifying an anomaly, additional surveys were performed at lines 3, line 3.5 (between line 3 and 4), and 4 (lines spaced 2 m apart) with a step size of 1 m. In case an anomaly is present, it should be seen in adjacent survey lines at similar spatial locations.

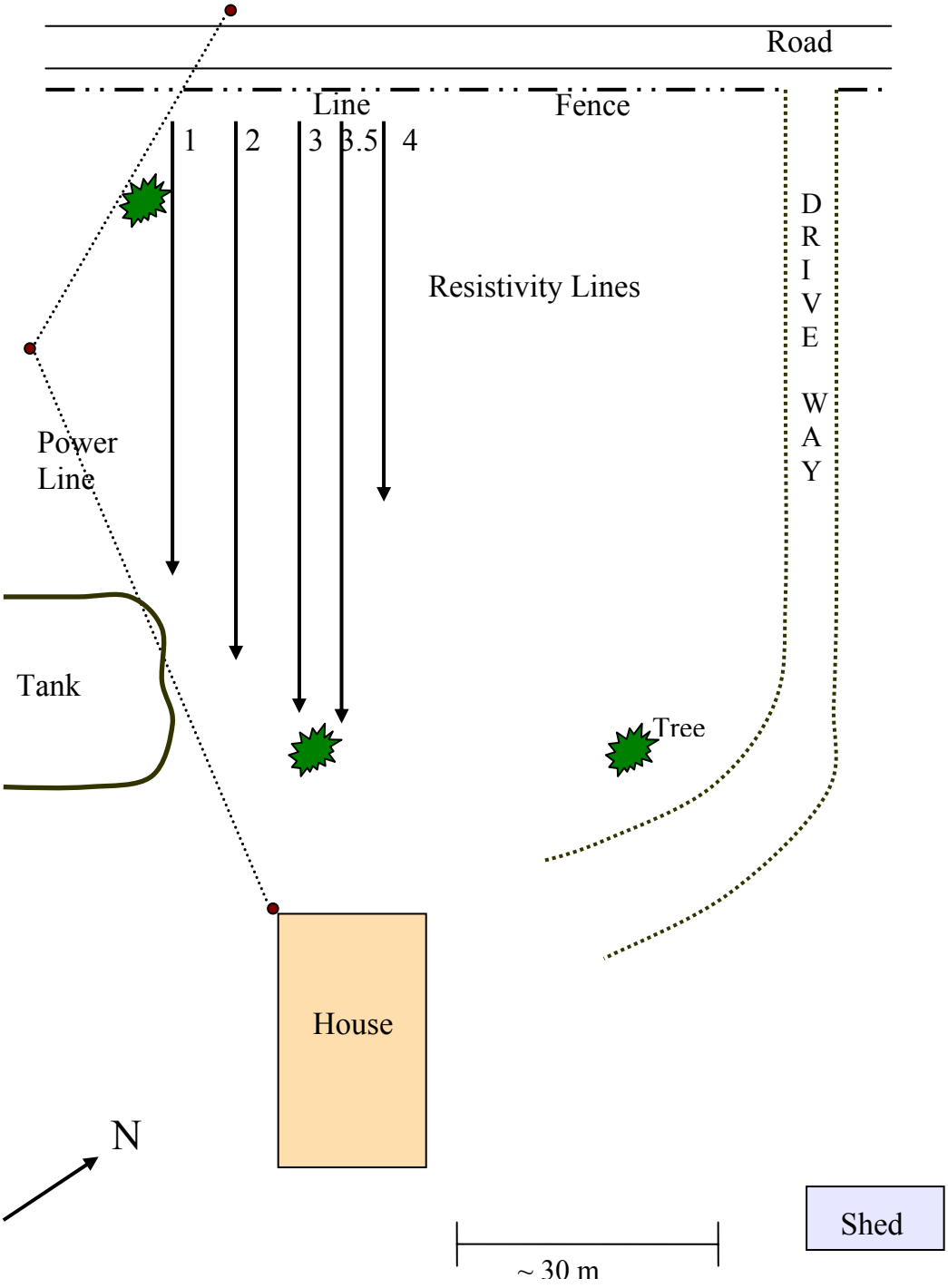

Fig. 35. Wenner resistivity survey setup at Bastrop.

Results

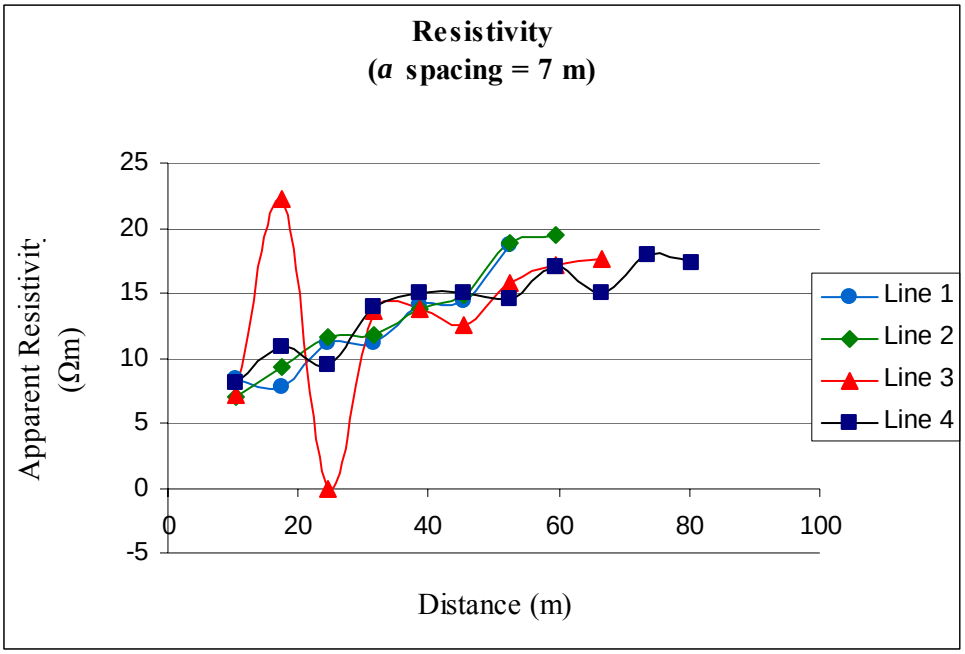

Fig. 36. Wenner resistivity survey for 4 lines with 'a spacing' = 7m (at Bastrop). Increasing resistivity as the survey moves away from the start position.

As seen in Fig. 36 the apparent resistivity increases with increasing distance from the start points of line 1 to 4 to the kidney-shaped open tank-like feature (see Fig. 35). Not much information can be derived from this set up since the step size is large (7 m), leading to the next surveys to be performed with a step size of 1 m.

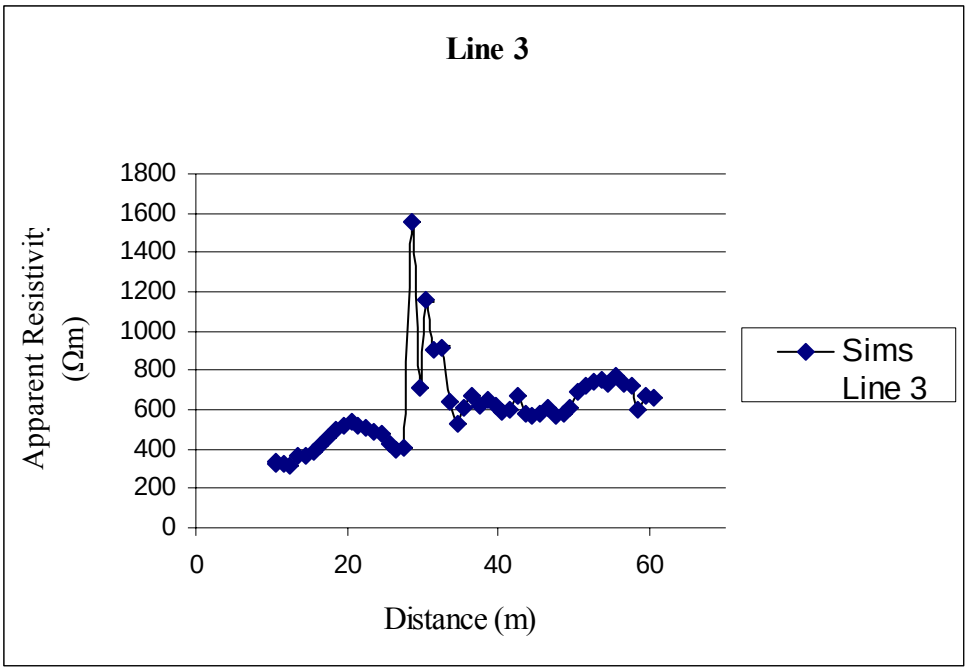

Fig. 37. Wenner resistivity survey along line 3 at Bastrop. Sudden spike seen at around 30 m from the start position.

Shown in Fig. 37, the apparent resistivity increases with increasing distance from start point of line 3. There exists a region of elevated apparent resistivity at around 30 m possibly because of some anomaly with high resistivity. If this anomaly is a void space related to coal mining, and is a continuous 3-D tunnel-like feature, then the higher resistivity of the cavity will also be detected in other survey lines adjacent to line 3.

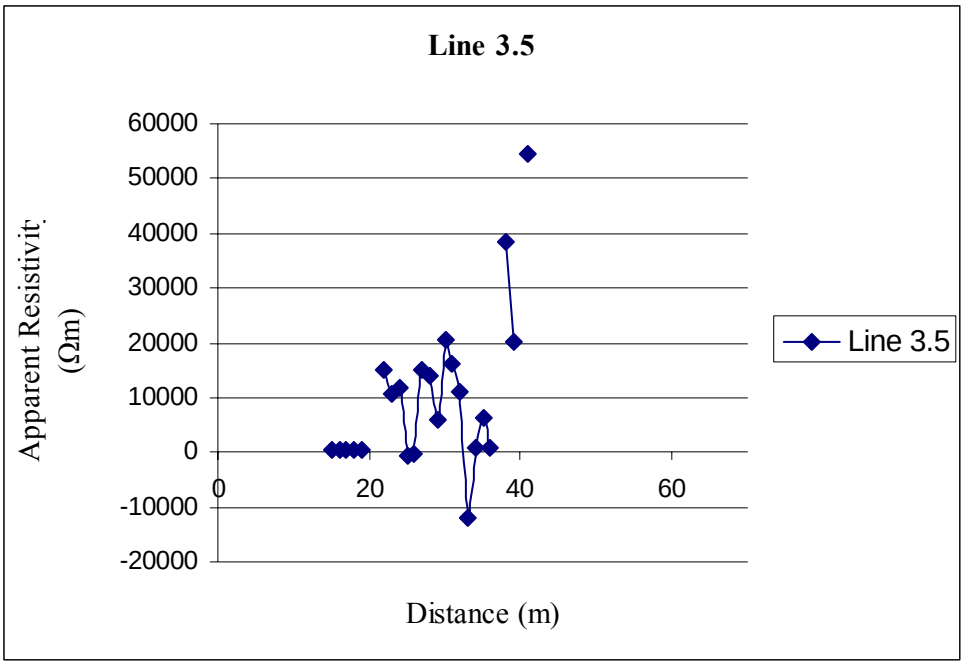

Fig. 38. Wenner resistivity survey along line 3.5 (between line 3 and 4) at Bastrop.

As seen in Fig 38 no specific trend is observed in line 3.5. During data collection, at some locations, no readings were measured by the instrument and hence the data are not continuous because of the highly resistive ground.

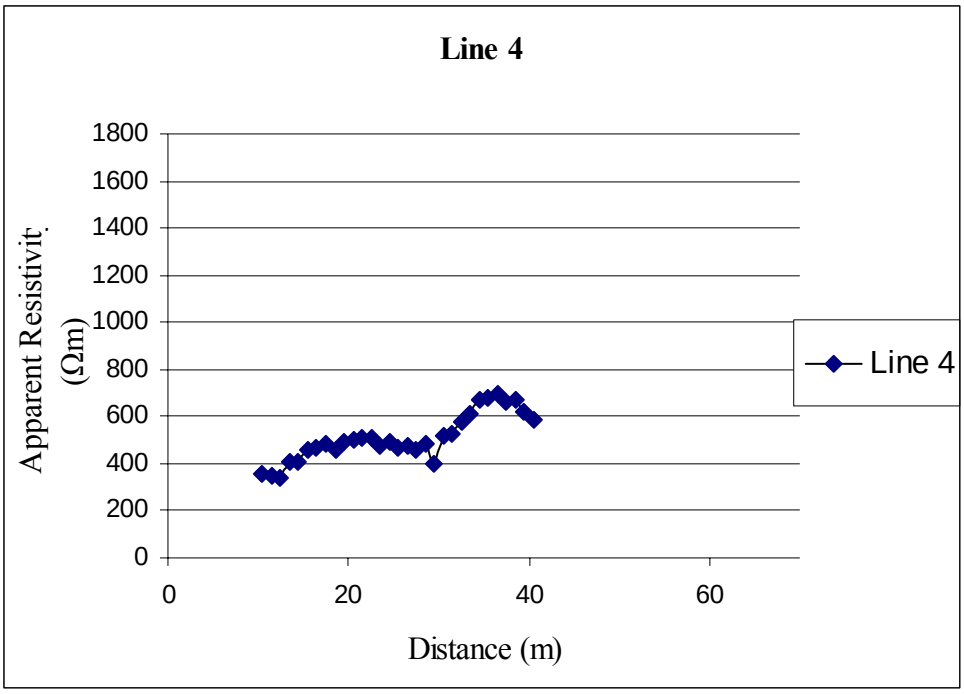

Fig. 39. Wenner resistivity survey along line 4 at Bastrop.

The data from line 4 (Fig. 39) indicates that there is an increase in the resistivity while moving away from the start point as in case of line 3 (Fig. 37). Though no sudden spike (increase in resistivity) observed in line 4, instead there is a small dip at 30 m.

Discussion

The surficial deposits at the survey are dominated by cobbles and pebbles, making it very difficult to ground the electrodes required for collecting the data. Also, the soil was very dry; such resistive conditions make data acquisition difficult. The survey area is also constricted and as a result few data could be obtained, which is unable to strongly support the GPR data. Decreasing the 'a spacing' would lead to a decrease in current penetration and hence decrease in the effective depth of penetration.

While gathering resistivity data, it was brought to our attention that the neighboring property (Area 2) had big sinkholes, a situation not observed at Area 1. These sinkholes were similar to those at Malakoff, but in a much more stable condition (visually). Hence, additional GPR data were collected at Area 2. Azimuthal surveys as in case of Malakoff were not possible since there were too many trees and shrubs at Area 2. These data are presented in Appendix A. About 1.6 km west of Area 1, fresh collapses are observed similar to ones seen at Malakoff. A previous study conducted by RRC indicated the existence of coal mining around the survey area. Owner of Area 2 conveyed that no new collapses or subsidence features have occurred on the property in the previous 15 years. At Area 1, there prevails extensive surface erosion, due to lack of vegetation. Repetition of anomalies (possible tunnels) occurrences on adjacent GPR survey lines in Area 1, stable sinkholes in Area 2 and surrounding regions, and historical background information indicates that this region was probably once a coal mining area. But, it is difficult to ascertain the exact nature and extent of coal mining related features at Bastrop without ground-truthing.

CONCLUSION

At Malakoff, one sinkhole was detected (JBR16), two roughly indicated (S5 & JBR19), 4 not accessible by backhoe (due to depth) or missed (not identified during reclamation) or anomaly not a mining related feature. Overall GPR technique using the azimuthal survey method was moderately successful in detecting coal mine related features at Malakoff. The tunnel-like features identified were filled with washed in sediments with different physical properties than the host soil surrounding it.

Several possible anomalies were identified before the ground truthing, but these were not necessarily located during the ground truthing done by RRC. A geophysical technique like GPR provides a pointer toward further investigation of the site survey. The reclamation at Malakoff was ground-truthing in a true sense, since false alarms were identified and shortcomings of the survey designs could be recognized. The occurrence of the tunnels found during reclamation in the near surface zone of the azimuthal GPR radargrams (for sinkhole S-5 and JBR-19) suggested the use of higher frequency (50 MHz and 100 MHz) antennae which, in turn, enabled the inspection of shallower regions of the subsurface (for sinkhole JBR-16 and NS). Multiple radii surveys around sinkhole NS with 50 MHz and 100 MHz antennae helped identify the anomaly with more confidence even without ground-truthing.

To begin with, data were collected along 9 linear survey lines. The location selected was a region lacking sinkholes within the area of inspection, but surrounded by sinkholes (S-4, S-5). The idea behind selecting this location was to identify any subsurface connection between these sinkholes. The linear surveys did suggest a

connection between the sinkholes, but no evidence was found in the azimuthal survey and the ground-truthing of sinkhole S-4 and S-5. In case of the multiple radii around sinkholes NS, a linear trend emanating out from the sinkhole could be identified. This suggests that a useful procedure would involve performing azimuthal surveys and following any anomaly heading away from the sinkhole. In theory, this cost effective procedure would lead to another sinkhole or location which might be in danger of collapse or subsidence. Also, all the anomalies found during ground-truthing were not at the same depth, which indicates that use of a single frequency GPR antenna may not be able to identify all tunnels/shafts. Multiple frequencies (GPR antennae) also help to reduce the false alarms, since varying the frequency can help confirm the existence of an anomaly due to repeatability.

The Bastrop survey area is a residential area, unlike the Malakoff site which is a ranch setting. Due to environmental/physical limitations (trees, fence etc) data acquisition was constrained affecting the resolution of data and increasing the cultural noise. Hyperbolae observed in various survey lines were observed at identical depths and relative positions, implying that they are probably produced by the same linearly trending anomaly. But this might not be the case always, and hence ground-truthing is important.

At Bastrop site Area 1, GPR anomaly exists at around 30m from fence line (start of survey) at a depth of around 9 m. A hazy appearance was seen in the near surface zone, indicating a disturbed soil zone above a collapsed anomaly, but this is difficult to ascertain without ground truthing. Supporting data for Area 1 at Bastrop are

necessary, especially since the site lacked physical/visual evidence (sinkholes, surface collapse features etc). Hence, a Wenner resistivity survey was performed at Area 1. The resistivity survey did identify some regions of high apparent resistivity. But each survey line varied distinctly with little co-relation and hence the apparent resistivity data were insufficient to derive definitive conclusions about the field site and to compare with the GPR survey. Further GPR survey was performed at Area 2 at Bastrop (property west of Area 1) to identify any possible tunnel like feature (data in Appendix A). Stable sinkholes, the presence of anomalies similar to Malakoff in the GPR data at Bastrop Area 2 and background information gathered lead to the conclusion that coal mining did occur in and around the vicinity of the field site at Bastrop. Since there hasn't been any major subsidence in the past decade in the two areas that were surveyed at Bastrop, the risk associated with the property is probably moderate to low. The data needs to be confirmed by ground-truthing. The property should be re-vegetated in order to reduce surficial erosion and washing off of the soil. The information obtained through GPR survey and the subsequent ground truthing, can be used by the property owners to better understand the risk associated with erection of major structures in close proximity to any possible coal mining related feature.

GPR data acquisition and processing is not very difficult and hence, GPR can be widely used for anomaly detection in industrial and research related fields like, environmental geosciences, engineering geology, archaeology, anthropology etc. Though, lack of experience in field survey set up, acquisition and interpretation can lead to increased false alarms. It was observed at Malakoff that the anomaly detection was

more successful when the survey design was altered and adapted to suit the geological and environmental constraints at the field site. The ground-truthing at Malakoff helped in making the required changes in the survey design to reduce the false alarm, thus indicating the importance of ground-truthing in developing geophysical investigation skills. In turn, the acquired geophysical data helped guide the reclamation. It can be concluded that GPR technique proficiently identifies anomalous coal mining related shafts/tunnels. Hence, extensive high quality GPR survey with a good survey design and under experienced supervision can reduce the time and cost of reclamation.

REFERENCES

Al-fares, W., Bakalowicz, M., Guerin, R., Dukham, M., 2002, Analysis of the karst aquifer structure of Lamalou area (Herault, France) with ground penetrating radar, Journal of Applied Geophysics, **51**, 97 - 106.

Batayneh, A. T., Abueladas, A. A., Moumani, K. A., 2002, Use of ground-penetrating radar for assessment of potential sinkhole conditions: an example from Ghor al Haditha area, Jordan, Environmental Geology, **41**, 977 – 983.

Beres, M. and Haeni, F. P., 1991, Application of ground-penetrating-radar methods in hydrogeology studies, Ground Water, **29**, 375 – 385.

Bhattacharya, P.K., and H.P. Patra, 1968, Direct current geoelectric sounding: Methods in geochemistry and geophysics, Elsevier Publishing Company.

Burger, H. R., 1992, Exploration geophysics of the shallow subsurface, Prentice-Hall, Inc.

Carreon-Freyre, D., Cerca, M., Hernandez-Marin, M., 2003, Correlation of near surface stratigraphy and physical properties clayey sediments from Chalco Basin, Mexico, using ground penetrating radar, Journal of Applied Geophysics, **53**, 121-136.

Chamberlain, A. T., Sellers, W., Proctor, C., Coard, R., 2000, Cave detection in limestone using ground penetrating radar, Journal of Archaeological Science, **27**, 957-964.

Church, R. H. and Webb, W. E., 1986, Evaluation of ground penetrating radar system for detecting subsurface anomalies, United States Department of the Interior, Bureau of Mines, Report of Investigation no. 9004, 21p.

Conyers, L. B., and Goodman, D., 1997, Ground-penetrating radar: An introduction for Archaeologist, Altamira Press.

Crowell, D. L., 2001, Mine subsidence, GeoFacts No. 12, Ohio Department of Natural Resources, Division of Geological Services, URL: http://www.dnr.state.oh.us/geosurvey/geo_fact/geo_f12.htm.

Davis, J.L., and Annan, A.P, 1989, Ground penetrating radar for high resolution mapping of soil and rock stratigraphy, Geophysical Prospecting, **37**, 531-551.

Dunrud, C. R., Osterwald, F. W., 1980, Effects of coal mine subsidence in Sheridan, Wyoming area, US Geological Survey Professional Paper, 1164, 49p.

Fisher, W. L., 1961, Stratigraphic names in the Midway and Wilcox groups of Gulf Coastal Plain, Gulf Coast Association of Geological Societies transactions, **11**, 263-295. Reprinted at University of Texas, Austin, Bureau of Economic Geology, Report of Investigation no. 44, 33p.

Fisher, W. L., 1963, Lignite of the Texas Gulf Coast Plain, Bureau of Economic Geology, Report of Investigation no. 50, 104p.

Friedel, M. J., Jessop, J. A., Thill, R. E., and Veith, D. L., 1990, Electromagnetic investigation of abandoned mines in the Galena, Kansas area, U.S. Bureau of Mines, Report of Investigation no. 9303, 20p.

Mathewson, C. C., Lacy, J., Davis, R. J., 1980, Texas Lignite, Texas Real Estate Research Center, Texas A&M University 16p.

Mellet, J.S., 1995, Profiling of ponds and bogs using ground-penetrating radar, Journal of Paleolimnology, **14**, 233-240

Powers, M. H., and Olhoeft, G. R., 1996, Modeling the GPR response of leaking, buried pipes, Symposium on the Application of Geophysics to Engineering and Environmental Problems, Colorado, 525-534.

Sharma, P. V., 1997, Environmental and engineering geophysics, Cambridge University Press.

Van Dam, R. L., Schlager, W., Dekkers, M. J., and Huisman, J. A., 2002, Iron oxide as a source of GPR reflection, Geophysics, **67**, 536-545.

Other Material Consulted:

Middleton, M. and Luppens, J. A., 1995, Geology and depositional setting of the lower Calvert Bluff Formation (Wilcox Group) in the Calvert Mine area, east-central Texas in Coal geology of the Paleocene-Eocene Calvert Bluff Formation (Wilcox Group) and the Eocene Manning Formation (Jackson Group) in east-central Texas, US Geological Survey Open-File report 95-595, URL: http://pubs.usgs.gov/of/1995/of95-595/index.htm.

National Coal Resource Assessment, USGS, URL: http://energy.er.usgs.gov/NCRA/Gulf_Coast_A.htm, September 16, 2004.

Railroad Commission of Texas Invitation for Bids for Malakoff Underground II Abandoned Mine Land (AML) site (FY 2003), Railroad Commission (RRC) of Texas, Surface Mining and Reclamation Division.

Strategic Center for Coal (Overview), National Energy Technology Laboratory, US Department of Energy (DoE), URL: http://www.netl.doe.gov/coal/overview.html, September 25, 2004.

Ulriksen, C.P.F. 1982: Application of impulse radar to civil engineering. Unpublished Ph.D dissertation, Lund University of Technology, Sweden.

Sensors and Software Inc. Technical manual, 1999, URL: http://www.sensoft.ca

Yancey, T. E., 1995, Depositional environment and stratigraphy of late Eocene sediments, east-central Texas in Coal geology of the Paleocene-Eocene Calvert Bluff Formation (Wilcox Group) and the Eocene Manning Formation (Jackson Group) in east-central Texas, US Geological Survey Open-File report 95-595, URL: http://pubs.usgs.gov/of/1995/of95-595/index.htm.

APPENDIX A

GPR at Bastrop Area 2

Lack of active coal mining subsidence features like the ones seen at Malakoff, lead to the investigation of the property located to the west of Bastrop survey area 1. Given below is a sketch of the survey set up (Fig. 40).

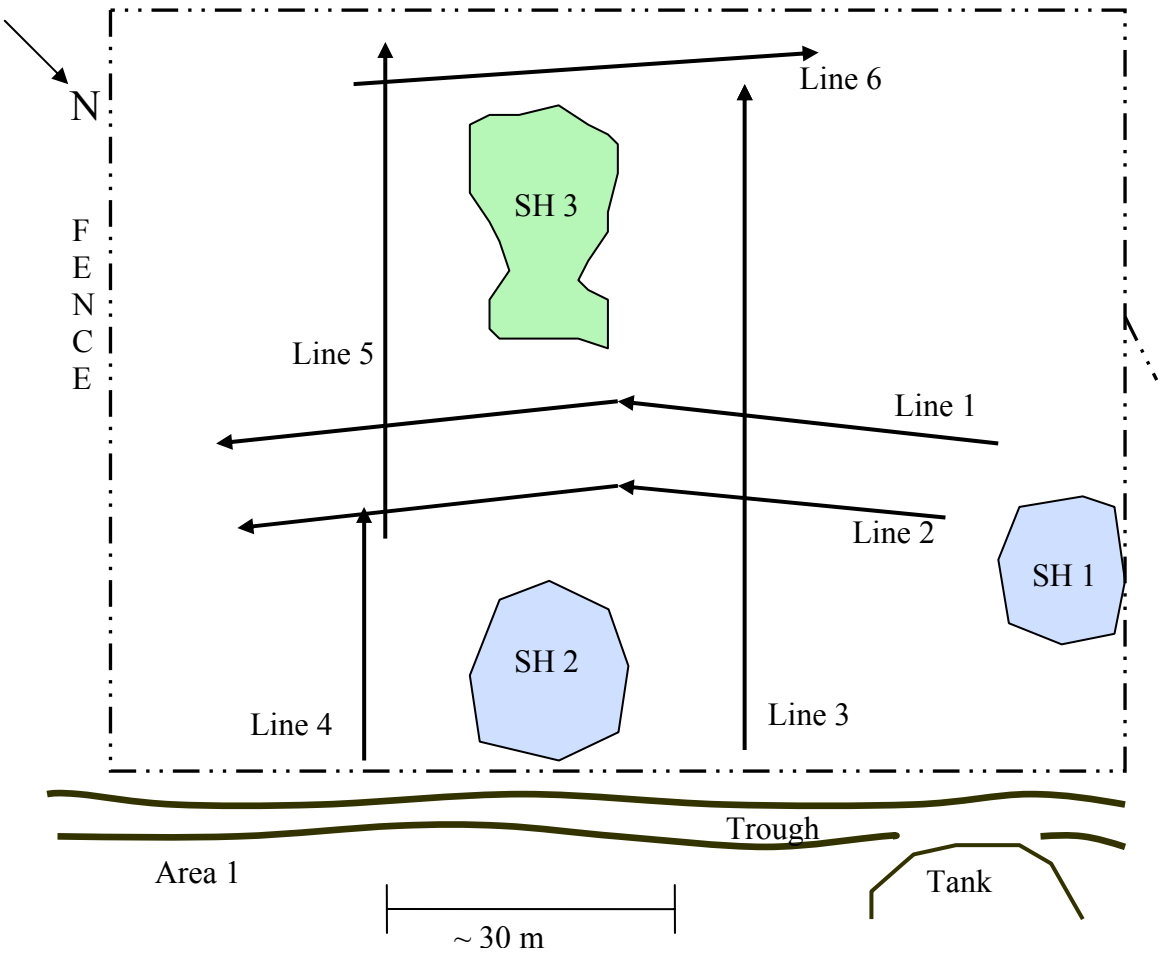

Fig. 40. GPR survey setup at Bastrop Area 2. Located adjacent to the survey Area 1.

Azimuthal survey could not be collected due to the heavy vegetation and lack of open space around the sinkholes. Linear common-offset reflection method was used to gather data in close proximity to the sinkholes. Two sinkholes (SH 1 and SH 2) are seasonally filled with water, and are known to be of depth ~5 m. Hence water table should be seen in the radar gram.

Results

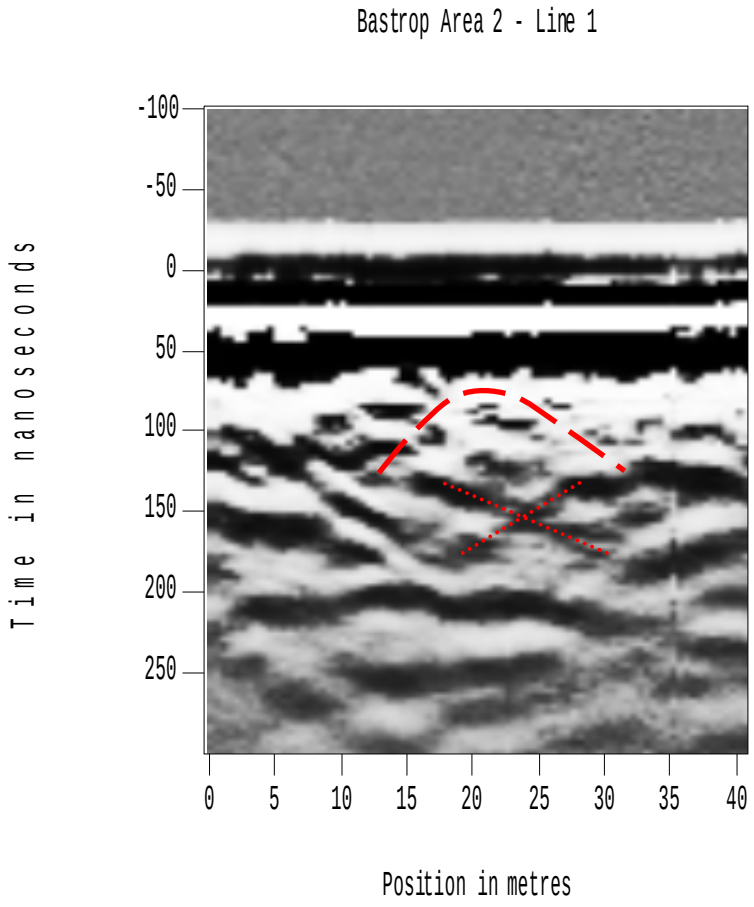

Fig. 41. Radargrams for line 1 at Bastrop (Area 2) using 25 MHz GPR.

Observation: Bow tie effect seen in the Fig. 41 above. Faint hyperbolae as seen at $\tau \sim$ 100 ns and at $x \sim 23$ m

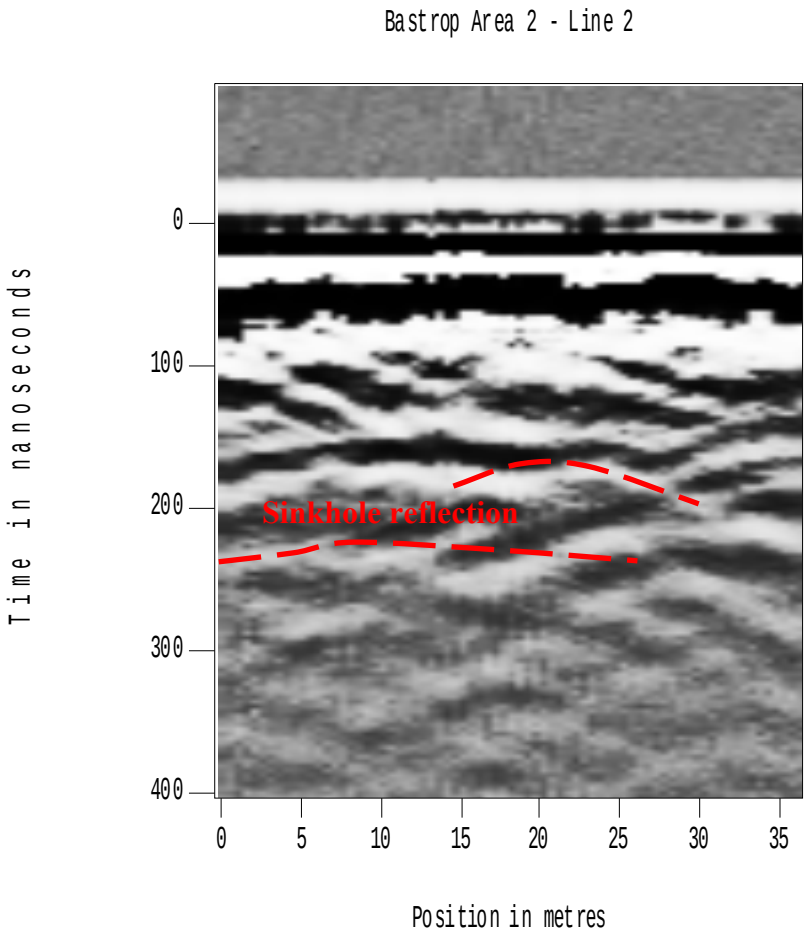

Fig. 42. Radargrams for line 2 at Bastrop (Area 2) using 25 MHz GPR.

Observation: At x ~20 m τ ~ 100 ns, a hyperbola is seen. Bow tie effect and multiples also observed. The relatively flat reflector is possibly the reflection of the sinkhole. A longer survey line would have enabled obtaining information about the reflector seen at the end of the radar gram.

Line 1 and Line 2 are parallel to each other with line 2 starting three m ahead of line 1. Hence, occurrence of a hyperbola at the same depth and relatively the same location from start position indicates a linear anomaly (oriented perpendicular to the lines).

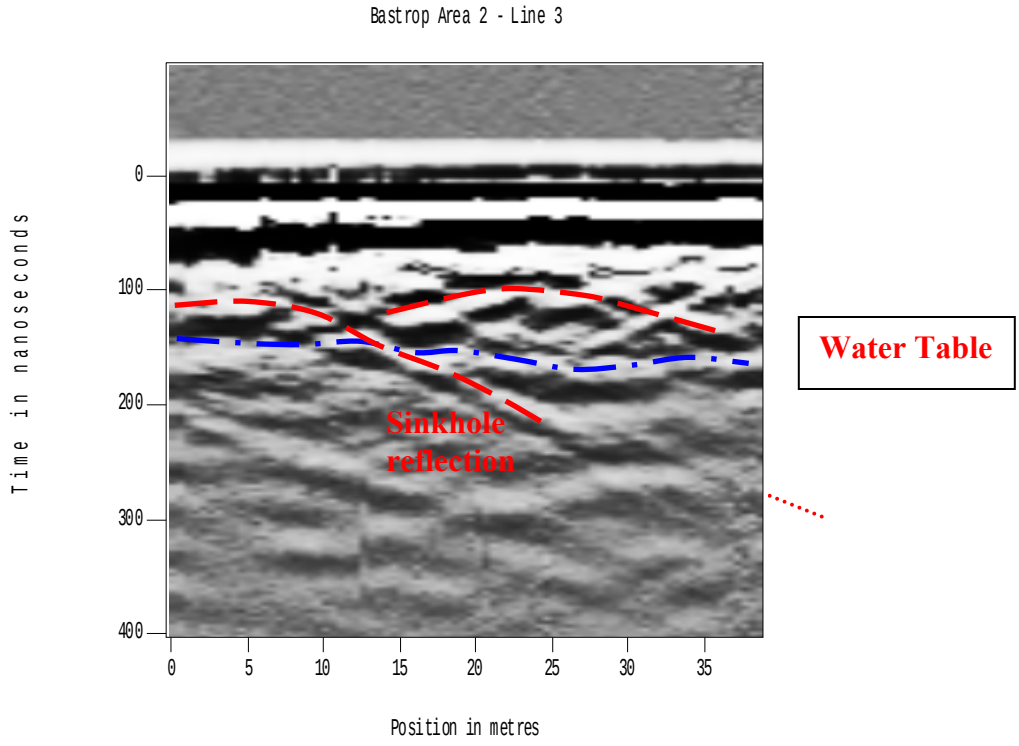

Fig. 43. Radargrams for line 3 at Bastrop (Area 2) using 25 MHz GPR.

Observation: Line 3 is very close to sinkhole SH 2 and crosses line 1 and line 2. Hyperbolae centering at $x \sim 25$ is seen.

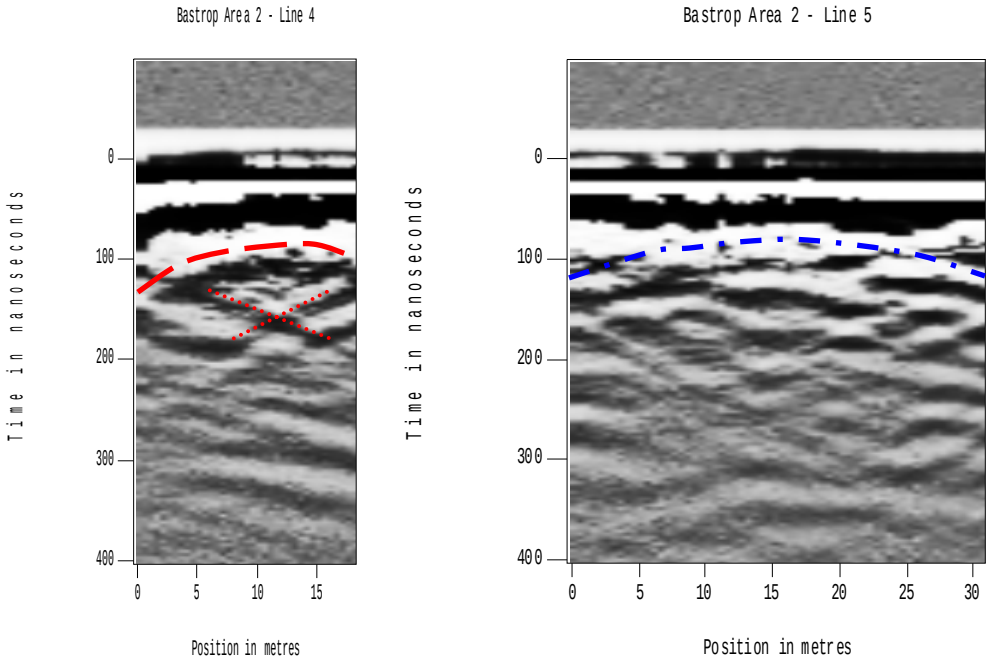

Fig. 44. Radargrams for line 4 - 5 at Bastrop (Area 2) using 25 MHz GPR.

Observation: Line 5 is a continuation of line 4 with a break and shift (survey line adjusted for the occurrence of trees and sinkholes). Bow tie effect below a hyperbola seen on line 4. Where as a possible water table can be seen in line 5.

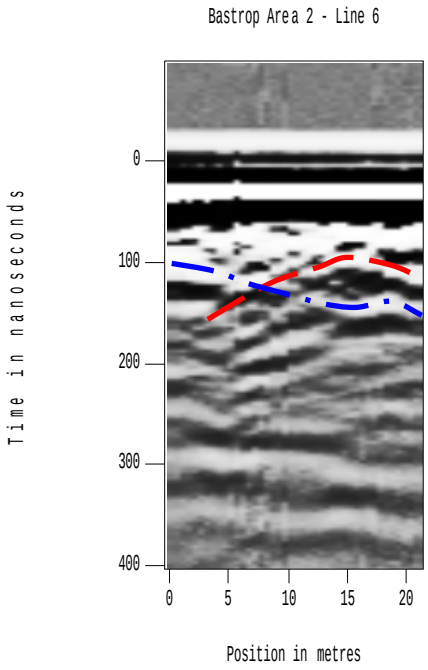

Fig. 45. Radargram for line 6 at Bastrop (Area 2) using 25 MHz GPR.

Observation: Line 6 is a short line and hence it is difficult to conclude much from it. There is no significant anomaly seen in the Fig. 45. The abrupt ending of the hyperbolae (due to the end of the line) and no adjacent data together makes the radar gram un-conclusive. Possible water table is seen in blue in Fig. 45. Since 25 MHz antennae were used, noise due to tree roots was eliminated because the signal produced by the roots occurred in the near surface zone

Discussion

The sinkholes at area 2 have been in existence for the past 15+ years with no major change in its structure. Two of the sinkholes fill up with water seasonally. Anomalies seen in the radargram for line 1 and 2 head towards the trough which lies in between Bastrop Area 1 and Area 2. This anomaly could possibly be connecting Area 1 to Area 2. Even though Area 2 was densely vegetated, using 25 MHz antennae lead to minimizing the effect of plant and tree roots since they occurred in the near surface zone. Ground-truthing is required to confirm the existence of coal mining in this region.

APPENDIX B

Table 5. GPR data collection key at Malakoff and Bastrop

Location	Survey Type	Sinkhole	Survey Name	Reclamation	Frequency (MHz)
Malakoff	Azimuthal	S-4	S-4	Pre	25
Malakoff	Azimuthal	S-5	S-5	Pre	25
Malakoff	Azimuthal	JBR-19	JBR-19	Pre	25
Malakoff	Azimuthal	JBR-16	JBR-16	During	100
Malakoff	Azimuthal	NS	NS-1	Post	50
Malakoff	Azimuthal	NS	NS-11	Post	50
Malakoff	Azimuthal	NS	NS-111	Post	100
Malakoff	Azimuthal	NS	NS-112	Post	100
Malakoff	Linear	-	NS-LN 1	Post	50
Malakoff	Linear	-	NS-LN 2	Post	50
Malakoff	Linear	-	Malakoff Line 1	None	25
Malakoff	Linear	-	Malakoff Line 2	None	25
Malakoff	Linear	-	Malakoff Line 3	None	25
Malakoff	Linear	-	Malakoff Line 4	None	25
Malakoff	Linear	-	Malakoff Line 5	None	25
Malakoff	Linear	-	Malakoff Line 6	None	25
Malakoff	Linear	-	Malakoff Line 7	None	25
Malakoff	Linear	-	Malakoff Line 8	None	25
Malakoff	Linear	-	Malakoff Line 9	None	25
Bastrop	Linear	-	Bastrop Area 1 - Line 1	None	25
Bastrop	Linear	-	Bastrop Area 1 - Line 2	None	25
Bastrop	Linear	-	Bastrop Area 1 - Line 3	None	25
Bastrop	Linear	-	Bastrop Area 1 - Line 4	None	25
Bastrop	Linear	-	Bastrop Area 1 - Line 5	None	25
Bastrop	Linear	-	Bastrop Area 2 - Line 1	None	25
Bastrop	Linear	-	Bastrop Area 2 - Line 2	None	25
Bastrop	Linear	-	Bastrop Area 2 - Line 3	None	25
Bastrop	Linear	-	Bastrop Area 2 - Line 4	None	25
Bastrop	Linear	-	Bastrop Area 2 - Line 5	None	25
Bastrop	Linear	-	Bastrop Area 2 - Line 6	None	25

Note: Data acquisition time period with respect to reclamation indicated by: pre (survey performed before reclamation), during (survey performed during reclamation), post (survey performed after reclamation) and none (reclamation not performed).

VITA

Neelambari Save
9 Ish Prasad, Andheri East
Mumbai 400069, India
Email: neelambari.save@gmail.com or
nsave@hotmail.com

EDUCATION

Texas A&M University, College Station, Texas — December 2004
Master of Science in Geophysics

Indiana University, Bloomington, Indiana — August 2002
Bachelor of Science in Geology, Minor in Mathematics

Sathaye College, Mumbai, India — May 1999
HSC Science Board

M. B. High School, Mumbai, India — May 1997
SSC Board